The Astrophysical Journal, 863:51 (18pp), 2018 August 10 https://doi.org/10.3847/1538-4357/aad087

An Expanded Gas-grain Model for Interstellar Glycine

Taiki Suzuki[1,2], Liton Majumdar[3], Masatoshi Ohishi[1,4], Masao Saito[1,4], Tomoya Hirota[1,4], and Valentine Wakelam[5]
[1] Department of Astronomy, the Graduate University for Advanced Studies (SOKENDAI), Osawa 2-21-1, Mitaka, Tokyo 181-8588, Japan; taiki.suzuki@nao.ac.jp
[2] Astrobiology Center, Osawa 2-21-1, Mitaka, Tokyo 181-8588, Japan; liton.majumdar@jpl.nasa.gov
[3] Jet Propulsion Laboratory, California Institute of Technology, 4800 Oak Grove Drive, Pasadena, CA 91109, USA
[4] National Astronomical Observatory of Japan, Osawa 2-21-1, Mitaka, Tokyo 181-8588, Japan
[5] Laboratoire d'astrophysique de Bordeaux, Univ. Bordeaux, CNRS, B18N, allée Geoffroy Saint-Hilaire, F-33615 Pessac, France
Received 2017 December 19; revised 2018 June 29; accepted 2018 June 29; published 2018 August 9

Abstract

The study of the chemical evolution of glycine in the interstellar medium is one of the challenging topics in astrochemistry. Here we present the chemical modeling of glycine in hot cores using the state-of-the-art three-phase chemical model NAUTILUS, which is focused on the latest glycine chemistry. For the formation process of glycine on the grain surface, we obtained consistent results with previous studies that glycine would be formed via the reactions of COOH with CH_2NH_2. However, we will report three important findings regarding the chemical evolution and the detectability of interstellar glycine. First, with the experimentally obtained binding energy from the temperature-programmed desorption (TPD) experiment, a large proportion of glycine was destroyed through the grain surface reactions with NH or CH_3O radicals before it fully evaporated. As a result, the formation process in the gas phase is more important than thermal evaporation from grains. If this is the case, NH_2OH and CH_3COOH rather than CH_3NH_2 and CH_2NH would be the essential precursors to the gas-phase glycine. Second, since the gas-phase glycine will be quickly destroyed by positive ions or radicals, the early evolutionary phase of the hot cores would be the preferable target for the future glycine surveys. Third, we suggest the possibility that the suprathermal hydrogen atoms can strongly accelerate the formation of COOH radicals from CO_2, resulting in the dramatic increase of formation rate of glycine on grains. The efficiency of this process should be investigated in detail by theoretical and experimental studies in the future.

Key words: astrochemistry – ISM: abundances – ISM: molecules – methods: numerical

1. Introduction

An attempt to understand the origin of life must necessarily begin with detailed studies of the formation and evolution of complex organic molecules (COMs), products of a complex chemistry that most likely starts in molecular clouds and continues within protoplanetary disks. However, the synthesis and evolution of organic molecules that form the building blocks of more complex biotic molecules is not well understood. There are two views regarding how COMs were formed on the early Earth: formation on the planetary surface, or exogenous delivery (Ehrenfreund et al. 2002).

In the interstellar medium (ISM), almost 200 molecules ranging from simple linear molecules to COMs were detected mainly toward dark clouds and low-mass and high-mass star-forming regions (as listed by CDMS[6]). Ehrenfreund et al. (2002) argued that the exogenous delivery of COMs to the early Earth by comets and/or asteroids could be as high as 1×10^{11} kg yr^{-1}, making it more important than their terrestrial formation by three orders of magnitude; thus, organic molecules delivered by extraterrestrial processes might have played a crucial role in early Earth chemistry. If this is the case, understanding the interstellar chemistry will enable us to better understand the first stage of chemical evolution regarding the origin of life: from atoms to very simple prebiotic species.

Since amino acids are the building blocks of life, the search for amino acids and their complex organic precursors at different stages of star and planet formation is one of the exciting topics in modern astronomy. Glycine (NH_2CH_2COOH), which is the simplest and the only nonchiral member out of 20 standard amino acids, was recently detected in the coma of comet 67P/Churyumov–Gerasimenko by the ROSINA (*Rosetta* Orbiter Spectrometer for Ion and Neutral Analysis) mass spectrometer (Altwegg et al. 2016), giving clues about glycine's interstellar origin. Several attempts have been made to detect glycine toward Sgr B2(N) and other high-mass star-forming regions, but none of them have been successful (e.g., Ceccarelli et al. 2000). Although Kuan et al. (2003) claimed the first detections of glycine toward high-mass star-forming regions, their detections were refuted by Snyder et al. (2005). While it is assumed that cometary glycine would be the remnant of the chemistry in a solar nebula (Walsh et al. 2014), its formation process in the ISM is still not well understood.

Many authors have discussed the formation processes of interstellar glycine. Blagojevic et al. (2003) assumed that glycine would be synthesized via ion–molecule reactions in the gas phase. They prepared some combinations of positive ions and neutral species and found that the reaction of "$NH_2OH^+ + CH_3COOH \longrightarrow NH_2CH_2COOH^+ + H_2O$" and "$NH_3OH^+ + CH_3COOH \longrightarrow NH_3CH_2COOH^+ + H_2O$" can efficiently form protonated glycine, which would be converted to the neutral form via dissociative recombination processes with an electron. Although NH_2OH (hydroxylamine) has not been detected in the ISM, it would be a plausible interstellar molecule since the ultraviolet laser irradiation of ice mixtures simulating interstellar grains produces hydroxylamine (Nishi et al. 1984). NH_2OH would be easily protonated in the gas-phase chemistry owing to its high proton affinity (Blagojevic et al. 2003). Charnley & Rodger (2005) performed chemical modeling calculation under the environment of hot cores with a constant density (10^7 cm^{-3}) and temperatures (100 and 300 K) through the simulations. Their simulations started from the

[6] https://www.astro.uni-koeln.de/cdms/molecules

observed or predicted interstellar ice abundances of CO, N_2, CH_4, H_2CO, C_2H_5OH, H_2S, C_2H_6, H_2O, CH_3OH, NH_3, HCOOH, and NH_2OH, as is found in Rodgers & Charnley (2001) in detail. They found that above ion–neutral processes in the gas phase can form glycine as much as 10^{-10} relative to molecular hydrogen.

The formation processes of glycine on interstellar grain surface have also been explored. Woon (2002) suggested that glycine would be built on the interstellar ice from COOH and CH_2NH_2 radicals. He assumed that the UV irradiation on H_2O/CO ice would lead to an abundant OH radical, which can react with CO to form a COOH radical. CH_2NH_2 can be formed via the hydrogenation process to HCN. Woon (2002) conducted quantum chemical calculations to show the activation barriers associated with "s-CO + s-OH" (here "s" represents species on the surface) and successive hydrogenation processes to HCN, which finally lead to CH_3NH_2. Later, Theule et al. (2011) confirmed CH_3NH_2 formation via a UV irradiation experiment on ice containing HCN and H atoms, implying that these processes would be valid in the ISM conditions. Then, Majumdar et al. (2013) used their hydrochemical model at 10 K to exclude the importance of the CH_2NH_2 + COOH reaction in such a low temperature.

Recently, Garrod (2013) investigated an effective formation route to glycine through chemical modeling. He assumed that grain surface radical–radical reactions would form glycine, for instance,

$$\text{s-COOH} + \text{s-CH}_2\text{NH}_2 \longrightarrow \text{s-NH}_2\text{CH}_2\text{COOH}, \text{ or}$$
$$\text{s-NH}_2 + \text{s-CH}_2\text{COOH} \longrightarrow \text{s-NH}_2\text{CH}_2\text{COOH}.$$

Garrod (2013) also considered the gas-phase formation of protonated glycine from CH_3COOH and NH_3OH^+ or NH_2OH^+, which were suggested by Blagojevic et al. (2003):

$$\text{NH}_2\text{OH}^+ + \text{CH}_3\text{COOH} \longrightarrow \text{NH}_2\text{CH}_2\text{COOH}^+ + \text{H}_2\text{O}$$
$$\text{NH}_3\text{OH}^+ + \text{CH}_3\text{COOH} \longrightarrow \text{NH}_2\text{CH}_2\text{COOH}_2^+ + \text{H}_2\text{O}.$$

The dissociative recombination process of $NH_2CH_2COOH_2^+$ with an electron in the gas phase will form glycine.

Under the fast warm-up model, which assumed the environment of high-mass stars where its timescale for the warm-up phase was assumed to be 7.12×10^4 yr, he found that the grain surface reaction, "s-COOH + s-CH_2NH_2 ⟶ s-NH_2CH_2COOH," was the most dominant formation route to glycine, and the effect of gas-phase formation routes is negligible. He claimed that s-COOH was formed via a photodissociation process of or a chemical hydrogen subtraction from s-HCOOH. In this case, the origin of s-COOH was not "s-CO + s-OH" as previously suggested by Woon (2002). s-CH_2NH_2 originates from the photodissociation of s-CH_3NH_2 in the solid phase, or hydrogen subtraction processes from s-CH_3NH_2 in the solid phase.

The first detection of interstellar glycine is the holy grail for astronomers. With the current capability of ALMA, which provides greater sensitivity and spatial resolution, glycine will be the prime target across different molecule-rich sources in the ISM. It is therefore invaluable to extend the state-of-the-art astrochemical models with the latest theoretical and experimental studies to simulate the glycine formation and its precursors in the ISM.

In this work, we investigate the importance of different glycine formation mechanisms and its detectability in hot cores using a newly developed chemical network implemented in the three-phase (gas surface mantle) NAUTILUS chemical model. The detailed descriptions of our chemical and physical models are discussed in Section 2. Our results are described in Section 3. Finally, we summarize our work in Section 4.

2. Chemical Model and Network

2.1. The NAUTILUS Chemical Model

To investigate the chemistry of glycine in hot cores, we have used the state-of-the-art chemical code NAUTILUS described in Ruaud et al. (2016). NAUTILUS allows us to compute the time evolution of chemical abundances for a given set of physical and chemical parameters. It simulates chemistry in three phases, i.e., gas phase, grain surface, and grain mantle. It also considers various possible exchanges among the different phases via adsorption of gas-phase species onto grain surfaces, the thermal and nonthermal desorption of species from grain surface into the gas phase, and the surface–mantle and mantle–surface exchange of species. A gas-to-dust ratio of 100 by mass, a grain density of 3 g cm^{-3}, and a grain radius of 10^{-5} cm were employed. Then, the total surface area was calculated assuming compact spherical grains. We modeled the standard interstellar UV radiation field and its destructions of molecules as was presented by Ruaud et al. (2016). Competition between reaction, diffusion, and evaporation is also taken into account in the model by following Chang et al. (2007) and Garrod et al. (2007). NAUTILUS computes diffusion energies of each species as a fraction of their binding energies and assumes a ratio of 0.4 for the surface and 0.8 for the ice mantle (see Ruaud et al. 2016, for more discussions). The thickness of the assumed barrier width is 1 Å that a surface species needs to cross while undergoing quantum tunneling to diffuse from one surface site to another. We have also updated the binding energy of each species in our model from Wakelam et al. (2017). The binding energy of a species is typically obtained by temperature-programmed desorption (TPD) experiments where either the temperature of the substrate is kept constant while the species of interest is deposited or the temperature is linearly increased until the species are desorbed from the substrate. Deposited species on the substrate can be in either the monolayer or multilayer regime. In the multilayer regime, desorption occurs from the species itself, and the impact of the underlying substrate becomes negligible as pointed out by Green et al. (2009). For glycine, the binding energy is estimated to be 13,000 K from Tzvetkov et al. (2004) (J.-C. Loison 2018, private communication). This experiment was performed in the multilayer regime, and so the effect of the substrate will have a minimal impact. Experiments in the monolayer regime are needed in order to quantify the mixing of the deposited glycine molecule with the water ice substrate. Nevertheless, we used the higher binding energy obtained by the TPD experiment as the extreme case to see the effect of binding energy on the gas-phase abundance of glycine.

To simulate the physical conditions in hot cores, we have used the two-stage physical model: free-fall collapse, followed by a dynamically static warm-up by following Garrod (2013). The cold collapse phase starts at $n_{H_2} = 3 \times 10^3\,cm^{-3}$ and moves to the final post-collapse density of $n_{H_2} = 2 \times 10^7\,cm^{-3}$. The increase in visual extinction during collapse leads to the minimum dust-grain temperature of 8 K followed by a warm-up from 8 to 400 K; during this phase, the gas and dust temperatures are assumed to be well coupled and the gas density is fixed. We assumed fast and slow warm-up models

Table 1
Initial Elemental Abundances Compared to Total Proton Density

Element	Abundance	Element	Abundance
H_2	0.5	Si^+	8.0 (−9)
He	0.09	Fe^+	3.0 (−9)
N	7.5 (−5)	Na^+	2.0 (−9)
O	3.2 (−4)	Mg^+	7.0 (−9)
C^+	1.4 (−4)	P^+	3.0 (−9)
S^+	8.0 (−8)	Cl^+	4.0 (−9)
F	6.7(−9)	…	…

Note. Elemental abundance used in our chemical reaction model.

described in Garrod (2013), whose timescales for the warm-up phases are 7.12×10^4 yr and 1.43×10^6 yr, respectively.

2.2. Developed Chemical Network for Glycine

To develop a state-of-the-art chemical network for glycine, we have started from the gas-phase chemical network kida.uva.2014[7] (Wakelam et al. 2015). It includes 489 species composed of 13 elements (H, He, C, N, O, Si, S, Fe, Na, Mg, Cl, P, F) linked with 7509 reactions. Garrod (2013) has adapted osu.2005 as an initial network to include the chemistry of glycine. We used similar elemental abundances to those from Garrod (2013), as listed here in Table 1. Also, we listed the binding energies used in our model in Table 2. The binding energies for some species were obtained by theoretical quantum chemical computation presented in Wakelam et al. (2017), but there are still some species whose binding energies were not measured or calculated. Our starting network includes various updates as compared to osu.2005 used in Garrod (2013). It considers the updates of HCN/HNC chemistry by Loison et al. (2014a), carbon chemistry by Loison et al. (2014b), branching ratios for reactions forming $C_{n=2-10}^{(0,+)}$, $C_{n=2-4}H^{(0,+)}$, and $C_3H_2^{(0,+)}$ from Chabot et al. (2013), and also various new data sheets available in the KIDA database. Our network for surface reactions and gas-grain interactions is based on the one from Garrod et al. (2007) with several additional processes from Ruaud et al. (2015). We have added the following updates into our initial gas-grain chemical network:

1. We have included the chemistry of glycine and other related COMs that are not available in the KIDA database from Garrod (2013).[8] This includes mainly four radical-addition reactions on the grains for glycine formation:

$$\text{s-NHCH}_2\text{COOH} + \text{s-H} \rightarrow \text{s-NH}_2\text{CH}_2\text{COOH} \quad (1)$$

$$\text{s-NH}_2 + \text{s-CH}_2\text{COOH} \rightarrow \text{s-NH}_2\text{CH}_2\text{COOH} \quad (2)$$

$$\text{s-CH}_2\text{NH}_2 + \text{s-COOH} \rightarrow \text{s-NH}_2\text{CH}_2\text{COOH} \quad (3)$$

$$\text{s-NH}_2\text{CH}_2\text{CO} + \text{s-OH} \rightarrow \text{s-NH}_2\text{CH}_2\text{COOH}. \quad (4)$$

These reactant radicals are mainly formed through either grain surface reactions or photodissociation of stable molecules. It also includes gas-phase destruction routes for glycine via UV photodissociation, either by the cosmic-ray-induced or standard interstellar radiation field or by ion–molecular reactions.

[7] http://kida.obs.u-bordeaux1.fr/
[8] http://www.astro.cornell.edu/~rgarrod/resources/

Table 2
Binding Energies of Key Species

Species	E_D (K)	Species	E_D (K)
(1) From Wakelam et al. (2017)			
H	650	C_2H_3	2800
H_2	440	C_2H_4	2500
C	10000	C_2H_5	3100
N	720	l-C_3H	4000
O	1600	c-C_3H	5200
CH_2	1400	HCO	1300
CH_3	1600	H_2CO	4500
CH_4	960	CN	2800
OH	4600	HCN	3700
H_2O	5600	HNC	3800
NH	2600	CH_3CN	4680
NH_2	3200	CH_3OH	5000
NH_3	5500	CH_3CH_2OH	5400
HOOH	6000	HNCO	4400
CO	1300	NH_2CHO	6300
CO_2	2600	CH_2OH	4400
CCH	3000	C_2H6	1600
C_2H_2	2587	CH_3O	4400
(2) Uncertain Values			
COOH	2000	CH_2NH_2	5530
NH_2OH	6810	CH_3CHO	5400
CH_3NH_2	6500	HNOH	5228
CH_3COOH	6300	CH_3NH	3553
$HCOOCH_3$	6295	CH_3OCH_3	3150
(3) Experimental Value			
NH_2CH_2COOH	13000		

Note. The binding energies for key species. (1) The binding energies for some species were given by the theoretical prediction described in Wakelam et al. (2017). (2) The species whose binding energy was guessed (e.g., Ruaud et al. 2015) owing to lack of both theoretical and experimental studies. (3) The binding energy of glycine was estimated based on the experiment by Tzvetkov et al. (2004).

The gas-phase reactions of CH_3COOH and protonated NH_2OH to form protonated glycine were also included from Garrod (2013), but the reaction rate coefficients of NH_2OH and its protonated species were updated from the theoretical calculation described in Barrientos et al. (2012).

2. We have updated the chemistry of CH_2NH and CH_3NH_2 from Suzuki et al. (2016). These reactions are a series of hydrogenation processes to HCN on grains, as summarized in Table 3.
3. We have included the glycine formation on the grains from Singh et al. (2013) via sequences of reactions with simple species, which are abundant in the ISM. They showed the following possible routes to form glycine via quantum chemical calculations:

$$\text{s-CH}_2 + \text{s-NH}_2 \rightarrow \text{s-CH}_2\text{NH}_2 \quad (5)$$

$$\text{s-CH}_2\text{NH}_2 + \text{s-CO} \rightarrow \text{s-NH}_2\text{CH}_2\text{CO} \quad (6)$$

$$\text{s-NH}_2\text{CH}_2\text{CO} + \text{s-OH} \rightarrow \text{s-NH}_2\text{CH}_2\text{COOH}. \quad (4)$$

While reaction (2) was employed in Garrod (2013), Singh et al. (2013) suggested the new reaction sequences to finally form glycine involving CH_2CO, NH_2CH_2CO, and NH_2CHCO. We tested the importance of these reaction sequences for the first time. Singh et al. (2013) concluded

that reactions (5) and (7) are barrierless reactions, while reaction (6) has an activation barrier of 7100 K.

Another sequence of reactions starts from a combination of NH_2 and CH, as below:

$$\text{s-NH}_2 + \text{s-CH} \rightarrow \text{s-NH}_2\text{CH} \quad (7)$$

$$\text{s-NH}_2\text{CH} + \text{s-CO} \rightarrow \text{s-NH}_2\text{CHCO} \quad (8)$$

$$\text{s-NH}_2\text{CHCO} + \text{s-OH} \rightarrow \text{s-NH}_2\text{CHCOOH} \quad (9)$$

$$\text{s-NH}_2\text{CHCOOH} + \text{s-H} \rightarrow \text{s-NH}_2\text{CH}_2\text{COOH}. \quad (10)$$

There are no activation barriers for reaction (7), (8), and (9). However, reaction (10) possesses an activation barrier of as high as ~37,000 K.

The third path starts from CH_2 and CO:

$$\text{s-CH}_2 + \text{s-CO} \rightarrow \text{s-CH}_2\text{CO} \quad (11)$$

$$\text{s-CH}_2\text{CO} + \text{s-OH} \rightarrow \text{s-CH}_2\text{COOH} \quad (12)$$

$$\text{s-NH}_2 + \text{s-CH}_2\text{COOH} \rightarrow \text{s-NH}_2\text{CH}_2\text{COOH}. \quad (2)$$

Reactions (11), (12), and (2) are barrierless reactions.

4. Based on the latest high-level quantum chemical computation from Barrientos et al. (2012), we have also included the following reactions in the gas phase: $NH_2OH_2^+ + CH_3COOH$ with a barrier of 1150 K, $NH_2OH^+ + CH_3COOH$ with a barrier of 12,180 K, and $NH_3OH^+ + CH_3COOH$ with a barrier of 13,600 K. The formation of the positive ion of glycine, $NH_2CH_2COOH_2^+$, will be followed by the dissociative recombination processes with an electron, to form glycine (~2%) and other fragmented species (~98%), such as NH_2, CH_2, and CH_2NH_2. All products and the reaction coefficients of these dissociative recombination processes were obtained from Garrod (2013), as summarized in Table 5 of Garrod (2013).

Finally,[9] we have nearly 4500 reactions on the grain surface linked with the 9500 reactions in gas phase.

3. Results and Discussion

3.1. The Chemical Compositions of the Grain Mantle during the Collapsing Phase

With our model, we calculate the evolution of fractional abundances compared to the total proton density (hereafter presented as X). In Figures 1(a) and (b), the fractional ice abundances of H_2O, CO, CO_2, CH_3OH, NH_3, CH_4, and H_2CO are shown. CO_2 is mainly formed from CO and O on grains. On the other hand, CO is formed in the gas phase and accretes on grains. The formation processes of H_2O, NH_3, CH_4, H_2CO, and CH_3OH are hydrogenation processes to O, N, C and CO, respectively, on the grain surface. In our model, water ice starts to form at 1×10^3 yr and shows its peak in between 2.005×10^8 yr and 2.025×10^8 yr. According to Ruaud et al. (2016), water ice reaches its peak in roughly 1×10^6 yr. This timescale is much shorter than our timescale of 1×10^8 yr. The main reason behind the different timescales is that Ruaud et al. (2016) assume a constant density of $1 \times 10^4\,\text{cm}^{-3}$, whereas our model assumed the time evolution during the collapsing phase. In our model, water ice shows its peak after 2×10^8 yr when density exceeds 1×10^4 cm^{-3}.

[9] The full chemical network is available on request to taiki.suzuki@nao.ac.jp and liton.majumdar@jpl.nasa.gov.

Table 3
Hydrogenation Processes to HCN Discussed in Suzuki et al. (2016)

Reaction	E_A (K)
$N + CH_3 \longrightarrow CH_2NH$	$E_A = 0$ K
$NH + CH_2 \longrightarrow CH_2NH$	$E_A = 0$ K
$NH_2 + CH \longrightarrow CH_2NH$	$E_A = 0$ K
$HCN + H \longrightarrow H_2CN$	$E_A = 3647$ K
$HCN + H \longrightarrow HCNH$	$E_A = 6440$ K
$H_2CN + H \longrightarrow CH_2NH$	$E_A = 0$ K
$HCNH + H \longrightarrow CH_2NH$	$E_A = 0$ K
$CH_2NH + H \longrightarrow CH_3NH$	$E_A = 2134$ K
$CH_2NH + H \longrightarrow CH_2NH_2$	$E_A = 3170$ K
$CH_3NH + H \longrightarrow CH_3NH_2$	$E_A = 0$ K
$CH_2NH_2 + H \longrightarrow CH_3NH_2$	$E_A = 0$ K

Note. The dust surface reactions related to CH_2NH and CH_3NH_2 are shown. E_A represents the value of the activation barrier. Since radical species are so reactive, radical–radical reactions would have no activation barriers. The activation barriers for HCN and CH_2NH were cited from the theoretical study by Woon (2002).

The molecular percentages compared to H_2O ice are plotted in Figures 1(c) and (d). We compare these molecular percentages in our model with Boogert et al. (2015) in Table 4. It is to be noted that observed ices toward massive YSOs are known to be slightly to strongly affected by thermal processing (Boogert et al. 2015). As a result, comparison of abundances of key ice species at the end of collapse may not be directly relevant for simulations run under the collapse model, i.e., where the dust temperature is as low as 16 K at the initial visual extinction of $Av = 2$, and during collapse this falls to a minimum temperature of 8 K, whereas gas temperature remains constant at 10 K. The best-fit age is 2.026×10^8 yr during the collapsing phase when the gas density gets high enough to form sufficient hydrogenated species via grain surface reactions.

3.2. Main Formation Routes to Glycine and Its Precursors

3.2.1. Fast Warm-up Model

In Figure 2(a), we show the fractional abundances of glycine calculated with the fast warm-up model (hereafter we refer it as the Fast Model). The abundances in the gas phase, on grain surface, and in the grain mantle are presented using the red, blue, and black lines. Once the peak abundance of glycine is achieved on grains, it starts to be destroyed through the grain surface reactions before glycine is thermally desorbed.

Figure 2(a) suggests that the peak abundance of glycine in the grain mantle is $\sim 1 \times 10^{-9}$ at $(4\text{–}5) \times 10^4$ yr since the beginning of the warm-up phase. In other words, the formation of glycine is completed on the grains at that time. In Figure 3(a), the formation rates ($\text{cm}^{-3}\,\text{s}^{-1}$) of glycine on the grain surface are compared. The most dominant formation path on the grains is "$\text{s-CH}_2\text{NH}_2 + \text{s-COOH}$," whose peak is achieved when the temperature is 60–120 K at $(4\text{–}5) \times 10^4$ yr. In the peak of black lines, the $HNCH_2COOH$ radical, which is produced via the destruction process of glycine, is used to reproduce glycine again via the hydrogenation process. Considering the fact that the abundance of glycine in the mantle achieved its peak at 5×10^4 yr, when "$\text{s-CH}_2\text{NH}_2 + \text{s-COOH}$" is the most efficient, this process would be the major path on the grain surface.

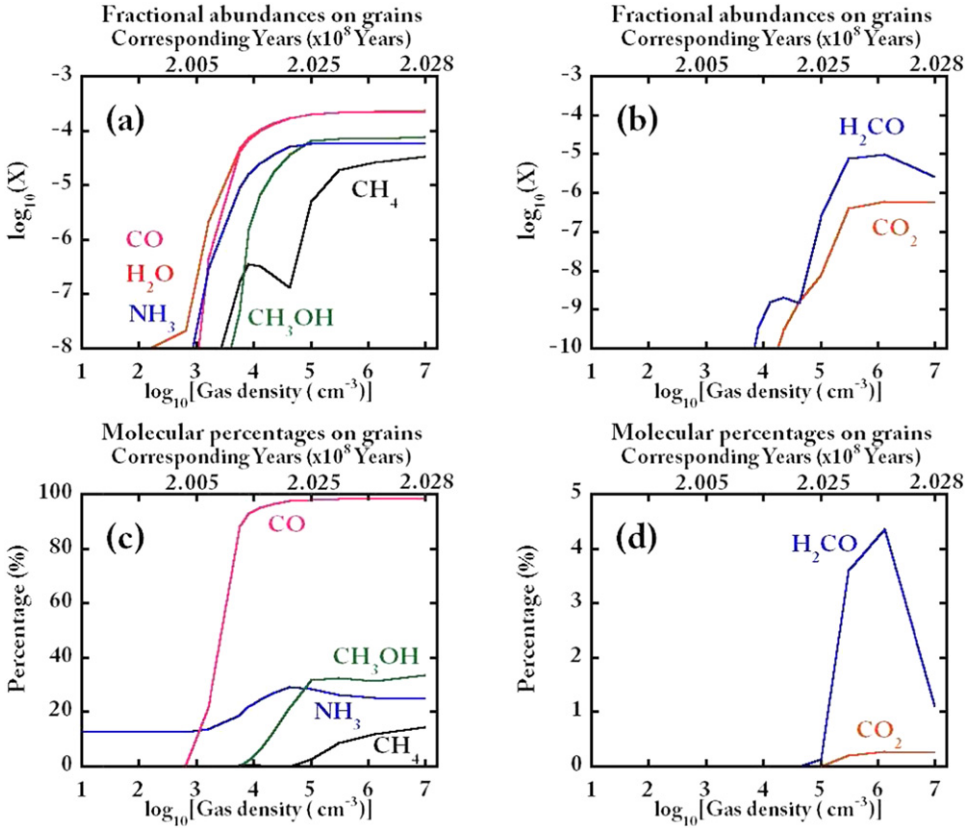

Figure 1. (a, b) Fractional abundance of H_2O, CO, CO_2, CH_3OH, NH_3, CH_4, and H_2CO in the solid phase, shown during the collapsing phase. (c, d) Molecular percentages compared to H_2O on grains.

Table 4
Comparison of Molecular Abundances on Icy Grains

	Best-fitting Time (yr)	H_2CO	CO	CO_2	CH_3OH	NH_3	CH_4	H_2CO
This work	2.026×10^8	100	98	0.2	32	26	9	4
LYSOs		100	4–14	12–25	5–23	∼7	1–3	∼2–7
MYSOs		100	12–35	23–37	5–12	4–8	3–6	∼6

Note. We show the best-fitted icy molecular abundances of basic species in our modeling at the end of the collapsing phase, compared to actual low-mass and massive young stellar objects (LYSOs and MYSOs) obtained by Boogert et al. (2015).

We plot the abundances of the glycine precursors CH_2NH_2 and COOH in Figures 2(b) and (c). The COOH radical is easily lost from the grain surface (blue dotted line) when the temperature is high (∼60 K). The formation rate of glycine on the grain surface via the "s-CH_2NH_2 + s-COOH" process decreases at $\sim 5 \times 10^4$ yr, when the COOH radical is completely lost from the grain surface. The formation rates of CH_2NH_2 and COOH radicals are compared in Figures 3(b) and (c), in a similar manner to glycine.

In Figure 3(b), we compare the formation rates of CH_2NH_2 via "s-CH_2NH + s-H ⟶ s-CH_2NH_2," "s-CH_3O + s-CH_3NH_2 ⟶ s-CH_3OH + s-CH_2NH_2," and the sum of the formation rates via other processes with green, red, and black lines, respectively. The process of "s-CH_2NH + s-H ⟶ s-CH_2NH_2" is efficient at the beginning of the warm-up phase, when the low temperature enabled the hydrogen atoms to be stored on grains. The other process, "s-CH_3O + s-CH_3NH_2 ⟶ s-CH_3OH + s-CH_2NH_2," is efficient when the temperature is more than ∼60 K, so that heavier radicals can move on the grain surface by thermal hopping. Since glycine is formed on the grains before 5×10^4 yr, the above two processes would be key origins of CH_2NH_2 radicals for the formation of glycine. The formation rates of the COOH radical are compared in Figure 3(c). The red line represents the formation rate of the COOH radical via the hydrogen subtraction process by H atoms from HCOOH: "s-H + s-HCOOH ⟶ s-H_2 + s-COOH." The green and blue lines, respectively, represent the sums of the formation rates of the COOH radical via destruction processes by NH_2 and OH radicals, respectively, of carboxyl groups, HCOOH, CH_3OCOOH, and $CH_2OHCOOH$. The former process was dominant when the temperature is low, while the latter processes are important when the grain surface temperature gets warmer and radicals can move on the grains. Figure 2(c) shows that the peak of the COOH radical on the grain surface is achieved at 3×10^4 yr, when the grain surface temperature is ∼30 K and the efficiency of "s-H + s-HCOOH ⟶ s-H_2 + s-COOH" decreases. Despite the efficient conversion process of HCOOH to COOH on grains at this age, the reverse hydrogenation process of "s-H + s-

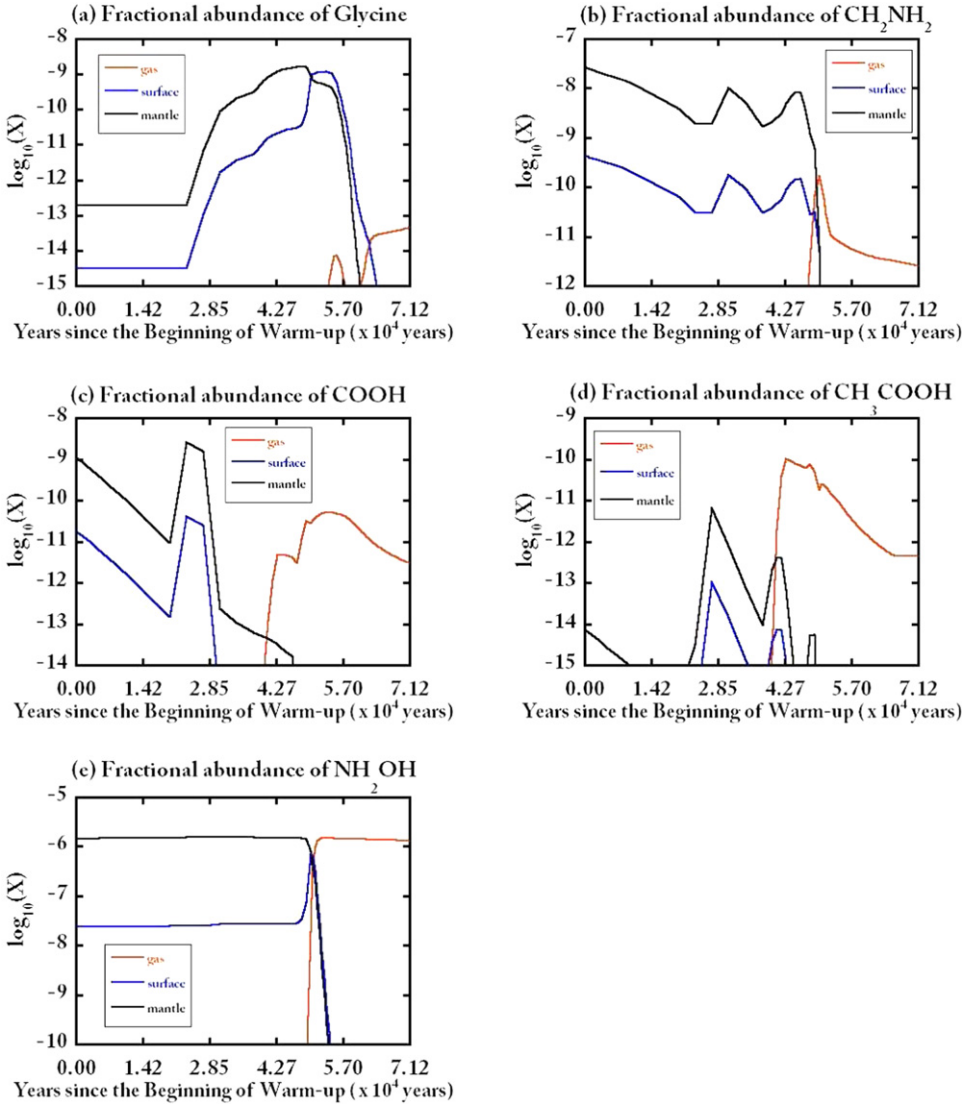

Figure 2. Simulated abundances of glycine and its precursors were compared using the Fast Model. The red, blue, and black lines, respectively, represent the abundances in the gas phase, on the grain surface, and in the grain mantle.

COOH $\longrightarrow$ s-HCOOH" suppresses the abundance of the COOH radical on the grains. Once hydrogen atoms are liberated from grains at 3×10^4 yr, the hydrogenation rate to convert the COOH radical to HCOOH decreases. As a result, the destruction processes of carboxyl groups by NH_2 and OH radicals increase COOH radicals on the grain surface. The above formation process of glycine on grains agrees with Garrod (2013).

Despite the agreement on the formation process of glycine on the grains with Garrod (2013), our chemical model suggests that the major formation process of gas-phase glycine is gas-phase reactions rather than the thermal evaporation of grains with its binding energy of 13,000 K, contrary to Garrod (2013). In Figure 3(d), we plot the subtraction of the accretion rate of gas-phase glycine from the evaporation rate of glycine on grains. The accretion rate always overwhelms the evaporation rate, suggesting that the thermal evaporation is not efficient. The comparison of the gas-phase formation rates of glycine in Figure 3(e) shows that "$NH_2CH_2COOH_2^+ + e^-$" is the major formation path to glycine at $\sim 5 \times 10^5$ yr since the beginning of the warm-up. $NH_2CH_2COOH_2^+$ is produced via the reaction of CH_3COOH and $NH_2OH_2^+$. $NH_2OH_2^+$ is formed from NH_2OH with the reactions of positive ions such as H_3^+ and H_3O^+, as shown in Figure 3(f). In our model, both CH_3COOH and NH_2OH are efficiently built on grains (Figures 3(g) and (h)). The formation of NH_2OH is almost completed during the collapsing phase. Once HNO is formed in the gas phase, it accretes on grains and was converted to NH_2OH via the hydrogenation processes. CH_3COOH is built on grains from CH_3CO and OH radicals. We conclude that the series of above reactions are the most essential process to form gas-phase glycine in this model. We note that the predicted abundances and the formation mechanisms discussed here are subject to the binding energies, reaction rates, and physical evolution of the core and should be updated based on the latest progress of these studies. Especially, the precise value of binding energy of glycine should be explored in detail in future works as the essential parameter to change the predicted glycine abundances, major formation processes, and key precursors.

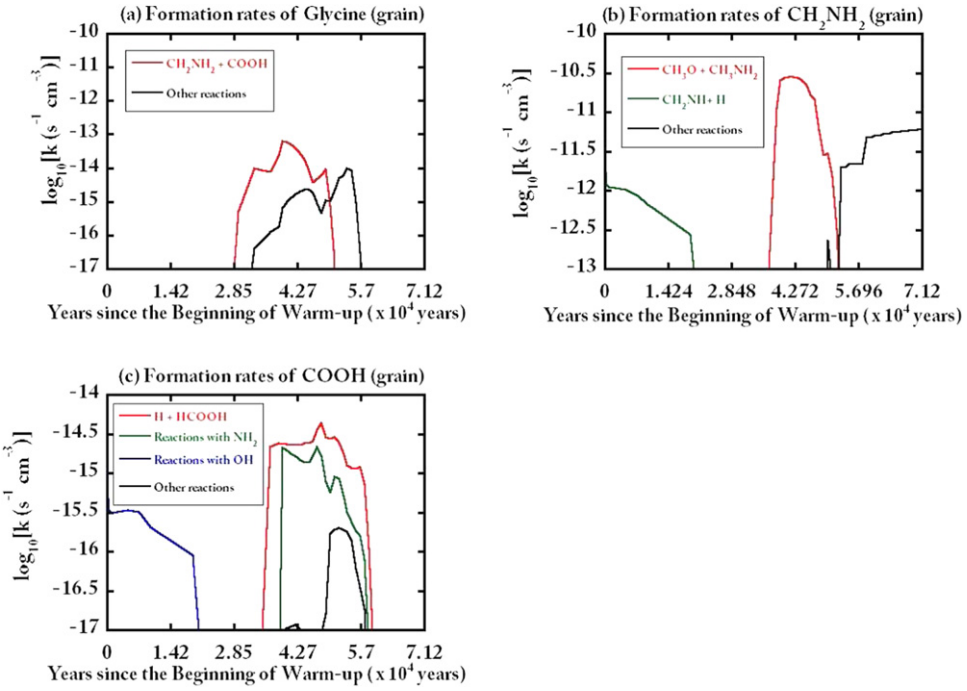

Figure 3. Formation rates ($cm^{-3}\ s^{-1}$) of grain surface reactions for glycine and its precursors were compared using the Fast Model. (a) Formation rates for glycine on the grain surface were compared. The red line corresponds to the "s-CH_2NH_2 + s-COOH" process, while the black line represents the sum of reaction rates for the other processes. (b) Formation rates for the CH_2NH_2 radical on the grain surface were compared. The red and green lines correspond to the "s-CH_3O + s-CH_2NH_2 ⟶ s-CH_3OH + s-CH_3NH_2" and "s-CH_2NH_2 + s-H ⟶ s-CH_2NH_2" process, respectively, while the black lines represent the sum of the reaction rates for the other processes. (c) Formation rates for the COOH radical on the grain surface were compared. The red lines correspond to the "s-H + s-HCOOH ⟶ s-H_2 + s-COOH" process. The green and blue lines represent the sum of the formation rates of COOH through hydrogen subtraction processes from HCOOH, CH_2(OH)COOH, and CH_3OCOOH by NH_2 and OH radicals, respectively. For instance, these processes are "HCOOH + NH_2 ⟶ NH_3 + COOH" or "CH_2(OH)COOH + NH_2 ⟶ NH_3 + H_2CO + COOH," and "CH_3OCOOH + NH_2 ⟶ NH_3 + H_2CO + COOH." It was assumed that they are the only products for the destruction process of HCOOH, CH_2(OH)COOH, and CH_3OCOOH. The black lines represent the sum of reaction rates for the other processes. The formation rates ($cm^{-3}\ s^{-1}$) of grain surface reactions for glycine and its precursors were compared using the Fast Model. (d) Subtraction of the accretion rate of gas-phase glycine from the evaporation rate of glycine on grains was plotted. (e) Formation rates for gas-phase glycine were compared. The red line represents the formation rates of glycine via the gas-phase reaction of "$NH_2CH_2COOH_2^+ + e^-$," while the black line represents the sum of the other reactions. (f) Formation rates of $NH_2OH_2^+$ were compared. The red, green, and blue lines, respectively, represent the reaction of NH_2OH with H_3^+, H_3O^+, and HCO^+. (g) Formation rates of NH_2OH were compared. The red line represents the subtraction of accretion rates of NH_2OH from that of evaporation rate, while the green line represents the sum of the formation rates of NH_2OH through the gas-phase reactions. (h) Formation rates of CH_3COOH were compared. The red line represents the subtraction of accretion rates of CH_3COOH from that of evaporation rate, while the green line represents the sum of the formation rates of CH_3COOH through the gas-phase reactions.

3.2.2. Slow Warm-up Model

In this subsection, we will present our results under the slow warm-up model, where the timescale of warm-up is 1.43×10^6. We show the simulated abundances and the formation route to glycine in Figures 4 and 5(a) in the same manner as the Fast Model. In this model (referred to as the Slow Model), the gas-phase peak abundance of glycine is much smaller than those on the grain surface and in the grain mantle. The peak abundance of glycine in the gas phase is lower than in the fast warm-up model, due to the destruction process on grains of glycine by radicals such as OH and NH before thermal evaporation.

In Figure 5(a), the formation rates ($cm^{-3}\ s^{-1}$) of glycine on grain surface are compared. The contributions of other reactions are mainly due to "s-H + s-$NHCH_2COOH$," where $NHCH_2COOH$ is formed via destruction processes of glycine. However, similar to the fast warm-up model, the most dominant process is "s-CH_2NH_2 + s-COOH," and its peak is achieved when the temperature is between 60 and 120 K at $(8–10) \times 10^5$ yr.

The abundances and the formation rates of the glycine precursors on grains, CH_2NH_2 and COOH, are compared in Figures 4 and 5(b) and (c) in the same way as the fast warm-up model. CH_2NH_2 is produced via the destruction processes of CH_3NH_2 by NH, OH, and CH_3O radicals. The formation process of COOH was the destruction of HCOOH, which is consistent with the fast warm-up model, while the destruction by UV photons is more important than the fast warm-up model owing to the longer timescale. For the overall trend, the formation process of glycine on the grains does not depend on the warm-up speed.

However, similar to the Fast Model, the fact that the accretion rate of glycine is higher than its evaporation rate (Figure 5(d)) suggests an efficient formation of this molecule in the gas phase. In the Slow Model, glycine is formed from the reaction of $NH_2OH_2^+$ with CH_3COOH (Figure 5(e)). $NH_2OH_2^+$ is formed from the gas-phase reactions of NH_2OH with positive ions, mainly H_3O^+ (Figure 5(f)). Both NH_2OH and CH_3COOH thermally evaporate during the warm-up phase (Figures 5(g) and (h)).

3.3. Comparison with Garrod (2013)

We report in Table 5 the gas-phase glycine abundance computed with our model and the one from Garrod (2013; Table 8). Similarly, the peak abundances (in the gas, in the surface, and in the mantle) of glycine precursors, NH_2OH, CH_2NH, CH_3NH_2, HCOOH, and CH_3COOH, in Garrod (2013) are shown in Tables 6 and 7, together with the temperature

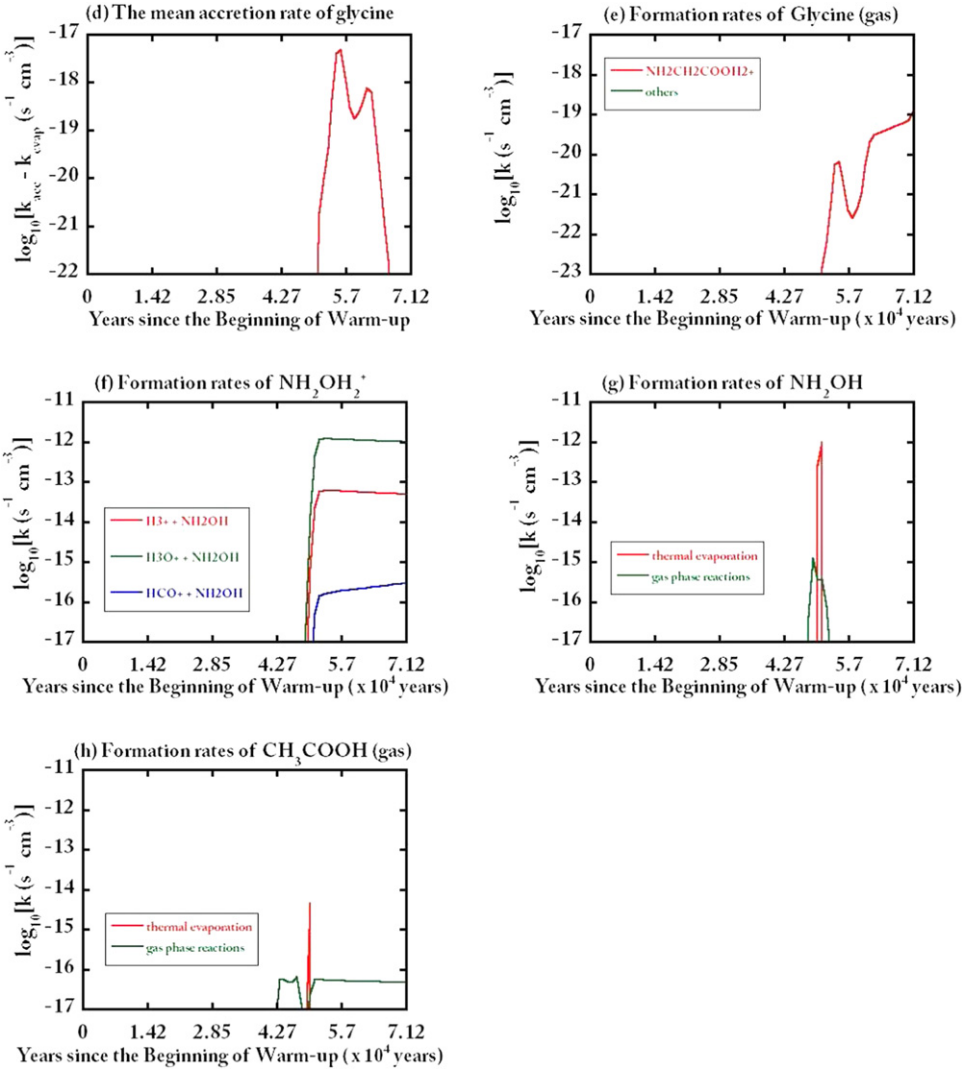

Figure 3. (Continued.)

corresponding to the peak. We note that we have only gas-phase abundances for the Garrod (2013) results. It is notable that the peak abundance of glycine was decreased by about a factor of 100 in our model as compared to Garrod. This discrepancy is due to the high desorption energy of glycine in our model, determined by the result of the TPD experiment by Tzvetkov et al. (2004). With the binding energy of 13,000 K, glycine is destroyed through grain surface reactions with NH or CH_3O radicals before it fully evaporates. The dramatic increase of NH_2OH and CH_3NH_2 in our model is due to the inclusion of a series of hydrogenation processes to NO and HCN, respectively. The increase of CH_2NH would be due to the update of gas-phase chemistry in kida.uva.2014, which is described in detail in Suzuki et al. (2016). In the Slow Model, CH_3COOH is depleted compared to Garrod (2013). Considering that this depletion is not seen in the Fast Model, the depletion is due to the longer timescale of the collapsing phase and the different amount of radical species to destroy CH_3COOH before its evaporation.

If the binding energy is 13,000 K, formation processes of glycine in the gas phase are more important than thermal evaporation from grains. The higher accretion rate than the evaporation rate shows the gas-phase origin of glycine (Figure 5(d)). In this case, glycine is formed via "$NH_2CH_2COOH_2^+ + e^-$," and the precursors are CH_3COOH and NH_2OH. These species are built on grains and then thermally evaporate into gas phase (Figures 4(d) and (e)).

We compare the abundances of glycine in the gas phase in Figure 6, changing the desorption energies of glycine to be 10,100 K, corresponding to the one in Garrod (2013). If we employ the same desorption energy as Garrod (2013) in the Fast Model (b), we obtain a peak abundance of gas-phase glycine of 3.1×10^{-11} for the fast warm-up model. This value agrees with Garrod (2013), where the peak abundance of glycine was reported to be 8.4×10^{-11}. These results clearly suggest that the discrepancy of the formation process of gas-phase glycine is due to the different binding energy of glycine, being the essential parameter to affect the abundance and the detectability of gas-phase glycine. With the binding energy of 10,100 K for glycine, the gas-phase abundance is mostly due to thermal evaporation.

These results strongly suggest that the binding energy of glycine is a key parameter that affects the abundance of gas-phase glycine. The further study of TPD experiments under the monolayer regime is required to improve our understanding further.

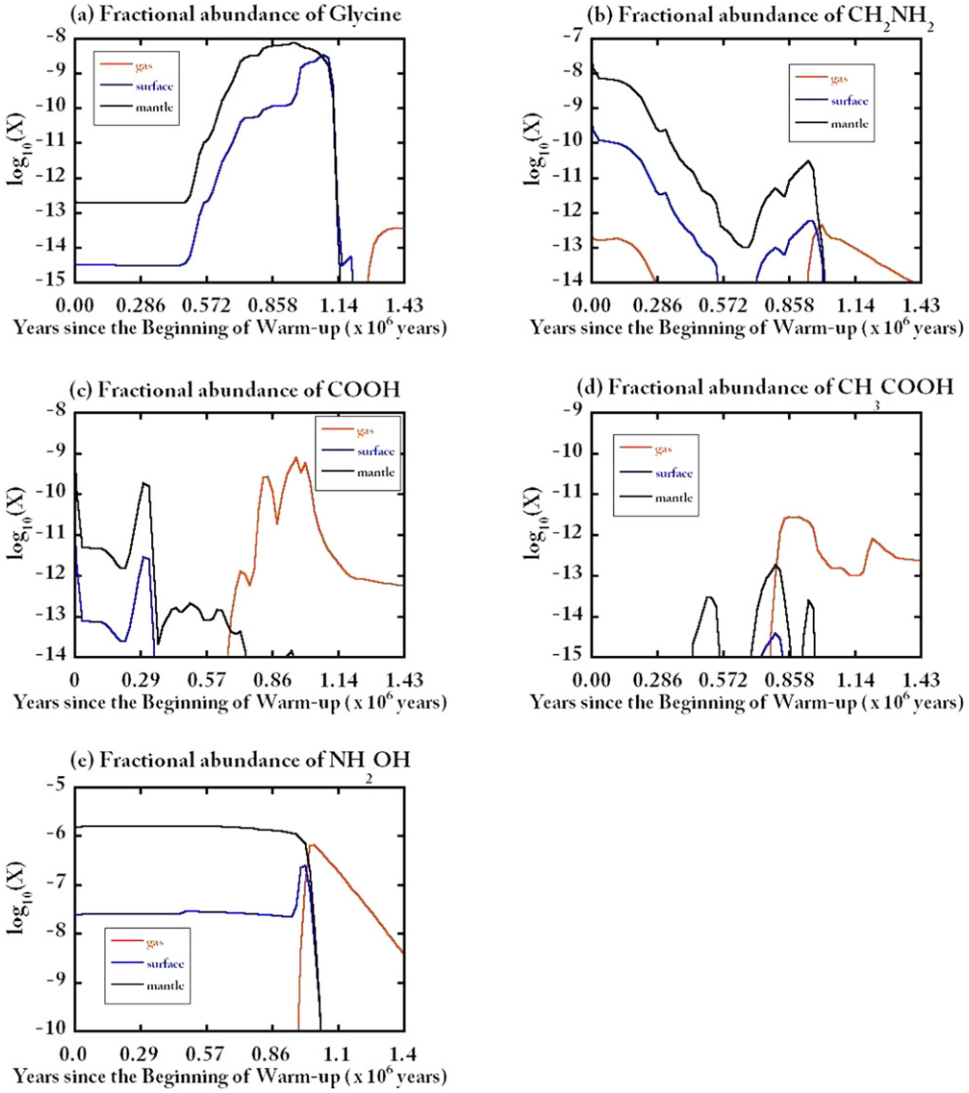

Figure 4. Simulated abundances for the Slow Model were shown in the same way as Figure 2.

3.4. Evaluation of the Simulated Abundance of Glycine

In this subsection, we will discuss whether the actual abundances of precursors of glycine can be explained with our Fast Model. Favre et al. (2017) detected CH_3COOH toward the edge of the Orion KL Hot Core and reported two velocity components with CH_3COOH column densities of 1.2×10^{16} cm^{-2} and 3.3×10^{15} cm^{-2}. Since the peak position of CH_3COOH is close to the source called HKKH7 reported in Hirota et al. (2015), we use the hydrogen column density of 1.1×10^{25} cm^{-2} based on the estimation by Hirota et al. (2015). Then, as summarized in Table 8, the fractional abundances of CH_3COOH in these components are, respectively, 1.0×10^{-9} and 3.0×10^{-10}. This value is close to $(0.9\text{–}7) \times 10^{-10}$, corresponding to that of Sgr B2 (Mehringer et al. 1997). With our peak fractional abundance of 1.0×10^{-10}, these values can be explained within a factor of 10. On the other hand, for NH_2OH, the upper limits of NH_2OH toward Orion KL and Sgr B2 are, respectively, 3×10^{-11} and 8×10^{-12} (Pulliam et al. 2012). These upper limits of NH_2OH suggest that we strongly overestimated the abundance of NH_2OH. Recently, Jonusas & Krim (2016) have experimentally shown that heating of NH_2OH–H_2O ices leads to a decomposition of NH_2OH into HNO, NH_3, and O_2 at 120 K, and it is possible that the lack of this effect may have led to strong overestimation of NH_2OH in our model. Since glycine is formed in the gas phase using the positive ion of NH_2OH, the gas-phase abundance of glycine would be overestimated and gives us only the upper limit. This result also suggests the importance of thermal decomposition processes of not only NH_2OH but also other species for the high-temperature chemistry.

On the grain surface, the important precursors are CH_2NH, CH_3NH_2, and HCOOH. As Suzuki et al. (2016) claimed that gas-phase CH_2NH would originate from the gas-phase reaction of "NH + CH_3," the gas-phase abundance of CH_2NH does not represent the grain surface origin of CH_2NH. Therefore, we will focus on HCOOH and CH_3NH_2 abundances in the gas phase for the benchmark of our calculation. Liu et al. (2002) reported the fractional abundance of HCOOH to be $\sim 3 \times 10^{-9}$ toward Orion KL, which agrees well with our peak value of 3.4×10^{-9}. However, our HCOOH abundance is higher than that of Sgr B2 (Ikeda et al. 2001), probably because the physical condition of Sgr B2 is different from our model. Pagani et al. (2017) reported the actual observation of CH_3NH_2 toward Orion KL to be 1×10^{16} cm^{-2}, corresponding to the fractional abundance of 1×10^{-9} assuming a hydrogen

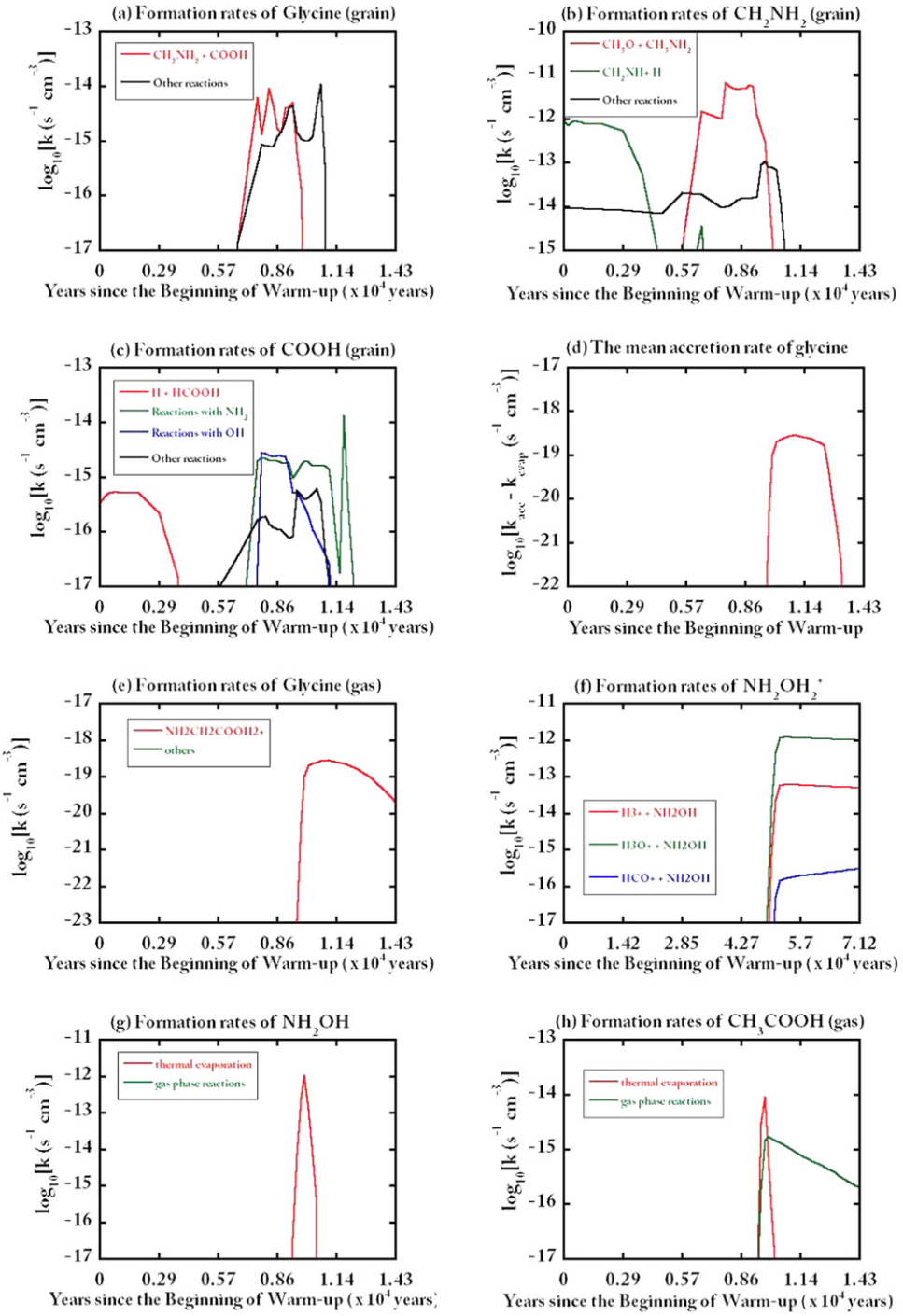

Figure 5. Formation rates (cm^{-3} s^{-1}) of grain surface reactions for glycine and its precursors were compared using the Slow Model. The formation rates (cm^{-3} s^{-1}) of grain surface reactions for glycine and its precursors were compared with the Fast Model in the same way as Figure 3. The labels denote the formation rates of (a) grain surface glycine, (b) grain surface CH_2NH_2, (c) grain surface COOH, (e) gas-phase glycine, (f) gas-phase $NH_2OH_2^+$, (g) gas-phase NH_2OH, and (h) gas-phase CH_3COOH. Panel (d) represents the subtraction of the accretion rate of gas-phase glycine from the evaporation rate of glycine on grains.

column density of 1.1×10^{25} cm^{-2} (Hirota et al. 2015). Halfen et al. (2013) reported similar CH_3NH_2 abundance of 1.7×10^{-9} toward Sgr B2. Since our peak abundance of CH_3NH_2 is 7.6×10^{-6}, we overestimated the abundance of CH_3NH_2 in the gas phase. This disagreement may be due to the fact that (1) hydrogenation processes to HCN and CH_2NH are not as efficient as we assume, and/or (2) the actual source age is $\sim 10^5$ yr after the completion of the warm-up and gas-phase CH_3NH_2 has already been destroyed in Orion KL. We will also assess the latter possibility in the subsequent section.

3.5. Future of Glycine Surveys in the Era of ALMA

The first detection of glycine is one of the biggest challenges in the field of radio astronomy. In this subsection, we will discuss the future detectability of glycine.

In Suzuki et al. (2017), we performed the chemical modeling study for high-mass star-forming regions, where we assumed that the temperature gradient inside hot cores would be represented by hot and warm temperature. While the temperature in the inner part of the hot core was set to be 200 K, the

Table 5
The Peak Abundances of Gas-phase Glycine in Different Models

Model	Eb (K)	X	T (K)
Garrod (2013)	10100	8.4 (−11)	216
Fast Model	13000	4.3 (−14)	400
Fast Model (b)	10100	3.1 (−11)	232

Note. The symbols Eb, X, and T, respectively, represent the binding energy of glycine used in the models, the peak of gas-phase fractional abundance of glycine, and the temperature when the peak abundance of glycine was achieved.

temperature of the outer region of the hot core was taken as a free parameter. We looked for the best combination of parameters in our modeling to explain the observed abundance of COMs, changing the age of the core, the temperature of warm region, and the volume ratio of the hot and warm region inside the hot core, using "the degree of proximity" from Wakelam et al. (2006) as a criterion to compare the modeling results with observed abundances. Through the comparison, we suggested that the ages of G10.47+0.03 and NGC 6334F were, respectively, 8×10^5 yr and 6.5×10^5 yr after the birth of the star, where chemical compositions were altered via the gas-phase reactions after the thermal evaporation. Hence, these ages would be reasonable to predict the abundances of glycine or other COMs in G10.47+0.03 and NGC 6334F, although Garrod (2013) stopped the chemical evolution just after the completion of the warm-up phase. In this subsection, we will simulate the chemical evolution up to 1×10^6 yr to compare with Suzuki et al. (2017), fixing the temperature and the density once the warm-up phase is completed.

We will use the Fast Model with the binding energy of 13,000 K for glycine. In Figure 7 we plotted the time evolution of the gas-phase abundance of glycine with the peak temperature of 400 K, along with the gas-phase abundances of CH_2NH, CH_3NH_2, NH_2OH, and CH_3COOH. The temperature of 400 K corresponds to the environment of the closer region to the central star and is more susceptible to stellar radiation than the 200 K region in Suzuki et al. (2017). We note that the gas-phase abundance of glycine is higher than that of Table 6, since the longer timescale enabled the gas-phase reaction of "$NH_2OH_2^+ + CH_3COOH$" to form protonated glycine, followed by the formation of glycine through the dissociative recombination with an electron. We plotted the time evolutions of glycine, CH_3NH_2, CH_2NH, NH_2OH, and CH_3COOH in Figure 7. Figure 7 implies that the abundances of glycine, CH_3NH_2, NH_2OH, and CH_3COOH will decrease over time owing to the destruction processes by positive ions and radicals. The gas-phase abundance of glycine between 6.5×10^5 yr and 8×10^5 yr was $\sim 10^{-14}$, lowered by one order of magnitude compared to its peak abundance.

Our modeling results suggest that the gas-phase abundance of glycine will be lowered by almost one order of magnitude after 5×10^5 yr since the beginning of the warm-up. Hence, the very early phase of the hot cores, where gas-phase destruction processes are less efficient, would be the ideal target sources to observe gas-phase glycine. We show the time evolutions of glycine and its precursors, NH_2OH and CH_3COOH, in Figure 7. Figure 7 tells us that NH_2OH and CH_3COOH can be used as the direct precursor to search for glycine-rich sources since they contribute directly in chemical kinetics of glycine in the gas phase and also follow similar evolutionary paths. We note that the number of sources of CH_3COOH is still limited. NH_2OH has not been detected in the ISM yet. Future survey observations of these species in the hot components will be helpful to constrain our chemical modeling. In addition, molecules built on grain surface, such as CH_3NH_2, can be used as the indicator of the early-phase hot core and hence potentially glycine-rich sources. They decrease with time via the destruction processes in the gas phase. By contrast, molecules originating in the gas-phase reactions, such as CH_2NH (Suzuki et al. 2016), do not show this trend. These species would also give us useful information regarding the age of the hot cores.

3.6. Comparison with Chemical Composition of Comet 67P from the Rosetta Mission

The comets are believed to be formed via the aggregation of interstellar dust particles within the protoplanetary disks, and the link between interstellar chemistry and the chemical compositions of comet is an interesting problem. The *Rosetta* mission reported many organic compounds in the coma of comet 67P/Churyumov–Gerasimenko. In the past, Biver et al. (2015) found a good agreement in cometary species and those in warm molecular clouds. This motivated us to compare our model predictions for glycine with the recent detection in comet 67P.

The recent detection of glycine by the *Rosetta* mission in 67P/Churyumov–Gerasimenko (Altwegg et al. 2016) implies that glycine would possibly be inherited from the parental cloud of our solar system. Altwegg et al. (2016) reported the detections of glycine in several positions, with its highest abundance ratio to water, "Glycine/H_2O," of 1.6×10^{-3}. Our fast and slow warm-up models developed for the high- and low-mass stars would give us some insights regarding the pristine chemical compositions preserved in the comets.

Comet are believed to have been formed via the accretion of interstellar dust particles. Considering that the large part of molecules would be frozen in the grain mantle rather than on the grain surface, the chemical composition of the grain mantle would be inherited by the cometary materials. We plotted the abundance ratio in the grain mantle of "Glycine/H_2O" in Figure 8 with green lines. While the evaporation rate for glycine is very low below 300 K owing to its high binding energy, H_2O is quickly lost compared to glycine. As a result, the ratio of "glycine/H_2O" has increased, and "glycine/$H_2O < 1.6 \times 10^{-3}$" is achieved when the temperature is less than 127 K. At that moment, the fractional abundances of glycine and water in the solid phase are, respectively, 9.4×10^{-10} and 6.9×10^{-7}.

3.7. Special Case: Glycine Chemistry with Suprathermal H^*

3.7.1. The Background of Suprathermal H^*

Muñoz Caro et al. (2002) conducted laboratory experiments and confirmed 16 amino acids, including glycine, after UV irradiation on ice containing H_2O, CH_3OH, NH_3, CO, and CO_2. Their experiments suggested that the formation of glycine is possible without HCN. However, the detailed formation mechanism was unclear at that time. To deepen the understanding of formation path to glycine in this scheme, Holtom et al. (2005) conducted experiments assuming a cosmic-ray-inducing environment on the interstellar ice analog containing CH_3NH_2 and CO_2, under the assumption that CH_3NH_2 would

Table 6
The Peaks of the Simulated Abundances for the Fast Warm-up Model in the "Garrod (2013) Model" and the Fast Model

	Garrod Model		Fast Model					
	Gas		Gas		Surface		Mantle	
Species	X	T (K)	X	T (K)	X	T (K)	X	T (K)
NH_2OH	1.6 (−10)	145	1.5 (−6)	158	6.8 (−7)	132	1.5 (−6)	25
CH_2NH	1.1 (−8)	400	5.6 (−7)	400	1.0 (−9)	132	5.3 (−8)	10
CH_3NH_2	8.0 (−8)	114	7.4 (−6)	149	3.0 (−6)	132	8.3 (−6)	11
NH_2CH_2COOH	4.3 (−9)	123	4.6 (−14)	400	1.2 (−9)	163	1.6 (−9)	117
HCOOH	4.8 (−8)	123	3.4 (−9)	314	3.6 (−10)	10	2.2 (−8)	10
CH_3COOH	1.0 (−10)	134	1.0 (−10)	84	1.1 (−13)	25	6.7 (−12)	25

Note. The peak of the fractional abundances and the temperature of grains at that moment in the Fast Model were compared with those of the Garrod (2013) Model. The notation of "a (b)" represents a $\times 10^b$.

Table 7
The Peaks of the Simulated Abundances for the Slow Warm-up Model in the "Garrod (2013) Model" and the Slow Model

	Garrod Model		Slow Model					
	Gas		Gas		Surface		Mantle	
Species	X	T (K)	X	T (K)	X	T (K)	X	T (K)
NH_2OH	1.6 (−10)	145	6.8 (−7)	156	2.5 (−7)	139	1.6 (−6)	10
CH_2NH	1.1 (−8)	400	6.6 (−6)	338	1.0 (−8)	132	5.3 (−8)	10
CH_3NH_2	8.0 (−8)	114	2.6 (−6)	147	6.3 (−7)	132	8.3 (−6)	10
NH_2CH_2COOH	4.3 (−9)	123	3.6 (−14)	368	3.5 (−9)	173	7.3 (−9)	124
HCOOH	4.8 (−8)	123	2.6 (−8)	202	3.6 (−10)	10	2.2 (−8)	10
CH_3COOH	1.0 (−10)	134	2.8 (−12)	104	3.8 (−15)	76	1.8 (−13)	76

Note. The peak of the fractional abundances and the temperature of grains at that moment in the Slow Model were compared with those of the Garrod (2013) Model. The notation of "a (b)" represents a $\times 10^b$.

Table 8
Comparison of Abundances between Our Model and Actual Abundances

Source	NH_2OH	CH_3COOH	HCOOH	CH_3NH_2
Orion KL	<3 (−11) (a)	3–10 (−10) (b)	3 (−9) (c)	1 (−9) (d)
Sgr B2	<8 (−12) (a)	0.9–7 (−10) (e)	1 (−11) (f)	1.7 (−9) (g)
Fast Model	1.5 (−6)	1.0 (−10)	3.4 (−9)	7.4 (−6)

Note. We compared the peak gas-phase abundances of glycine's precursors, NH_2OH, CH_3COOH, HCOOH, and CH_3NH_2 in our model, with actual observed abundances toward star-forming regions. Since observations of these species have been performed toward high-mass stars, we used the Fast Model for this comparison. The notation of "a (b)" represents "a $\times 10^b$."
References. (a) Pulliam et al. 2012; (b) Favre et al. 2017; (c) Liu et al. 2002; (d) Pagani et al. 2017; (e) Mehringer et al. 1997; (f) Ikeda et al. 2001; (g) Halfen et al. 2013.

have formed from CH_3 and NH_2 radicals during the experiments by Muñoz Caro et al. (2002). As a result, they reported the detection of glycine. They claimed that this process starts from photo cleavages of C–H and N–H bonds in CH_3NH_2 and creates CH_2NH_2 and H. Although a grain surface process of "s-CO_2 + s-H ⟶ s-COOH" is not likely to occur owing to its high activation barrier of 65.6 kJ mol^{-1} (∼7900 K; Zhu et al. 2001), the nascent H atom by strong UV photons would have extra energy to overcome this barrier (Holtom et al. 2005; Lee et al. 2009). The reaction "s-CH_2NH_2 + s-COOH ⟶ s-NH_2CH_2COOH" has no entrance barrier (Holtom et al. 2005). Furthermore, Lee et al. (2009) reported the formation of glycine from CH_3NH_2 and CO_2 on interstellar ice analog films under UV irradiation at 7.3–10 eV, corresponding to the effective energy range for interstellar UV radiation. We note that Garrod (2013) also claimed the importance of the reaction of "s-CH_2NH_2 + s-COOH ⟶ s-NH_2CH_2COOH." However, he assumed that COOH was formed from the subtraction of an H atom from HCOOH by radicals such as OH, rather than the hydrogenation process to CO_2.

Two sources of UV photons would be available to form H^* in actual star-forming regions. The first possibility would be the blackbody emission from the central star. However, we deduce that this process is important in only a limited region through the following calculation with the assumption of a spherical symmetric sphere.

It is known that Av is proportional to the hydrogen column density: N[H] (cm^{-2}) = 2.21 × 10^{21} Av (mag) (Güver & Özel 2009). According to the density profile based on the observations and theoretical studies of UCHII regions by Nomura & Millar (2004), the hydrogen atom number densities (n_H) are not so different within 0.1 pc. With a peak density of 1 × 10^7 cm^{-3}, we are able to calculate Av by using the distance from the star "r" as follows:

$$Av = 1.4 \times 10^4 \times r(\mathrm{pc}). \quad (13)$$

In NAUTILUS, the photodissociation rates are presented by the formula below with Av:

$$k = A \exp(-CAv)\ \mathrm{s}^{-1}. \quad (14)$$

The coefficients A and C can be theoretically and/or experimentally obtained. In this case, the photodissociation

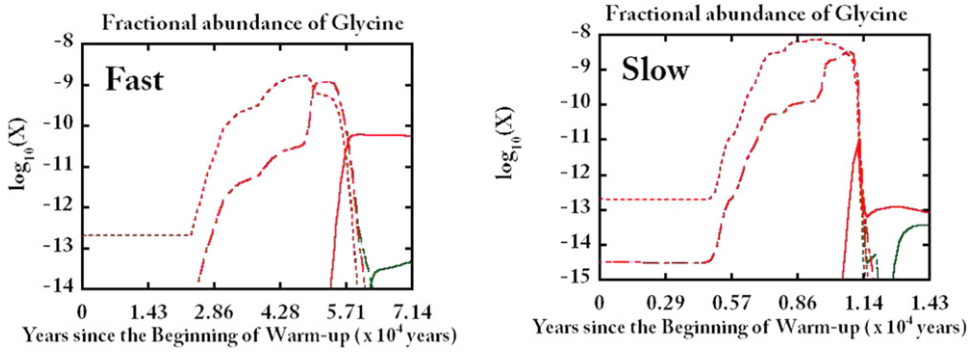

Figure 6. Simulated abundances of glycine under the different desorption energies. The solid, dot-dashed, and dotted lines, respectively, represent the abundances in the gas phase, on the grain surface, and in the grain mantle. The green and red lines correspond, respectively, to the cases of the desorption energy of 13,000 and 10,100 K.

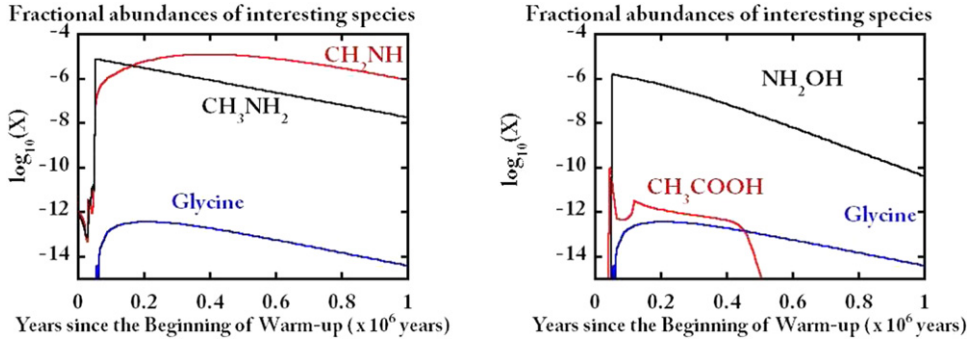

Figure 7. Time evolution of gas-phase abundances of glycine, CH_3NH_2, CH_2NH, NH_2OH, and CH_3COOH plotted with the Fast Model. The gas-phase abundances of glycine, CH_3NH_2, NH_2OH, and CH_3COOH are decreased among the gas-phase reactions with positive ions and radicals, whereas CH_2NH is still kept in high abundance. Our observations of COMs indicated that G10.47+0.03 and NGC 6334F would have ages between 6.5×10^5 yr and 8×10^5 yr (Suzuki et al. 2017).

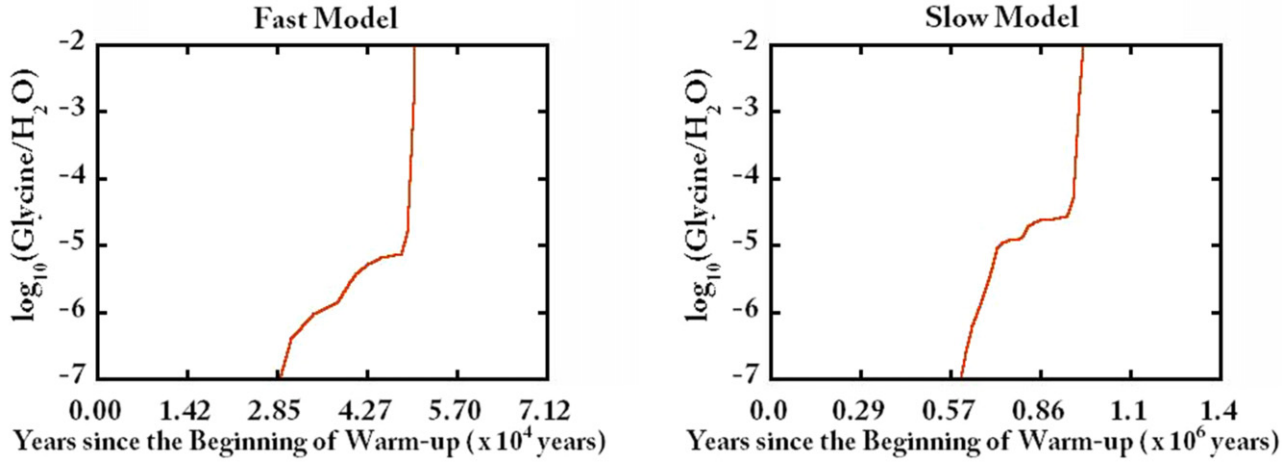

Figure 8. Time evolution of the abundance ratio "Glycine/H_2O" on the grain mantle using the fast and slow warm-up models. For both cases, the ratio was increased along with the warm-up of the core, since the evaporation of H_2O began at much lower temperature than glycine.

rate will decrease by a factor of $\sim 8.3 \times 10^{-7}$ by every 0.01 pc. Since the UV photons from the star would be available only in a limited region, we do not employ the star as the source of UV photons.

The other possibility for the source of UV photons is related to the cosmic rays. Prasad & Tarafdar (1983) suggested that the cosmic rays are an important source of UV flux in dense regions with large Av, where interstellar UV photons cannot penetrate. These mechanisms are included in kida.uva.2014. For the modeling of H^*, we simply assumed that H^* is created by the dissociation process of any H-bearing species by a UV field by the Prasad–Tarafdar mechanism instead of H.

For instance,

$$\text{s-}CH_3NH_2 + h\nu \longrightarrow \text{s-H}^* + \text{s-}CH_2NH_2, \text{ or}$$
$$\text{s-}NH_3 + h\nu \longrightarrow \text{s-H}^* + \text{s-}NH_2.$$

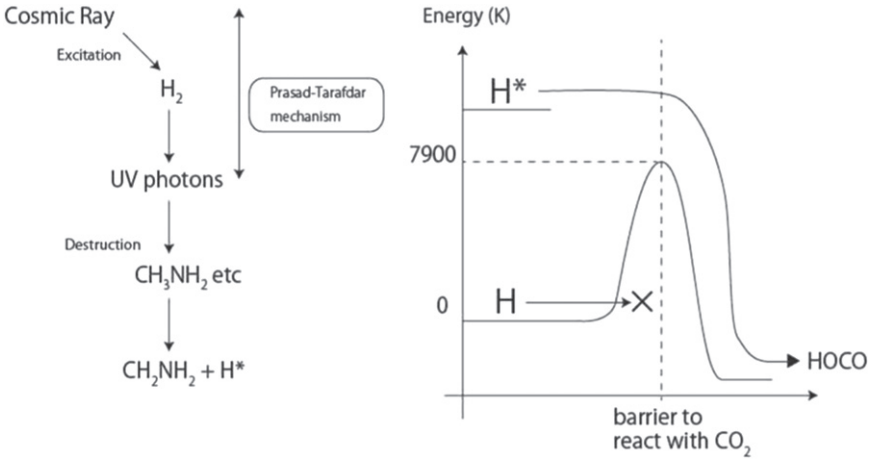

Figure 9. It was assumed that suprathermal hydrogen is formed via the UV radiation field. In dense cores, the UV radiation field would be formed by the Prasad–Tarafdar mechanism, starting from the destruction of H_2 by cosmic rays. When such a UV radiation field destroys molecules, dissociated hydrogen atoms would have extra energy and are referred to as "suprathermal hydrogen" H^*. Although it is unlikely for usual H atoms to react with CO_2, the extra energy of H^* makes it possible to overcome the activation barrier.

The activation energy for the grain surface reaction, "s-CO_2 + s-H ⟶ s-COOH," is ∼7900 K (0.68 eV). When UV photons with their energy of above 5 eV destroy CH_3NH_2, ∼4.3 eV is used to dissociate the C–H bond, and extra energy is given to the dissociated hydrogen atoms that can sufficiently overcome the potential barrier associated with the "s-CO_2 + s-H" process. Since all grain surface reactions in our model have lower activation barriers than "s-CO_2 + s-H ⟶ s-COOH" ($E_A \sim 7900$ K), H^* would be able to overcome any activation barriers associated with grain surface reactions in our model. Therefore, we develop a new model referred to as the "Fast + H^* Model," where H^* can lead to any hydrogenation process by penetrating activation barriers ($E_A = 0$ K). For instance, not only "s-CO_2 + s-H^* ⟶ s-COOH" but also other grain surface hydrogenation processes such as "s-CO + s-H^* ⟶ s-HCO" are treated as barrierless reactions. We present a diagram of formation paths of H^* and COOH in the above scenario in Figure 9.

For simplification, other chemical properties for H^* were assumed to be the same as the usual H atoms. It was assumed that H^* acts as a usual H atom in the gas-phase chemistry after the evaporation process.

The inclusion of H^* changes the reaction rates of hydrogenation processes dramatically. Recall that reaction rates on grains are proportional to κ_{ij}, as is given in the below formula using activation energy E_A:

$$\kappa_{ij} = \exp(-2(a/\hbar)(2\mu E_A)^{1/2}), \quad (15)$$

where "a" is the rectangle barrier of thickness (1 Å) and μ is the reduced mass. κ_{ij} is 2.7×10^{-16} for the usual hydrogenation process to CO_2 (s-H + s-CO_2 ⟶ s-COOH), with its activation energy of ∼7900 K. With such a low reaction rate, the usual hydrogenation process to CO_2 would be negligible even if CO_2 is abundant. However, κ_{ij} becomes unity for hydrogenation processes of H^*, where $E_A = 0$. The conversion of CO_2 to COOH by the hydrogenation process of H^* may strongly change the abundances of COOH on grains.

We also added the conversion processes of H^* to usual hydrogen atoms:

$$\text{s-H}^* + \text{s-H}^* \longrightarrow \text{s-H}_2,$$
$$\text{s-H}_2 + \text{s-H}^* \longrightarrow \text{s-H}_2 + \text{s-H, and}$$
$$\text{s-H} + \text{s-H}^* \longrightarrow \text{s-H}_2.$$

Finally, we note that we neglect the thermalization process of H^* in our model. According to the theoretical study of Andersson & van Dishoeck (2008), the H atom following the UV photodissociation can move tens of angstroms before the thermalization due to interactions with H_2O ice. Although the timescale of thermalization and chemical reaction of H^* is not well known, it is thought that the timescale chemical reaction should be longer than this thermalization process (Cuppen & Walsh 2017). Therefore, our model may overestimate the effect of H^*, and the impact of thermalization process for the chemical evolution has to be deeply investigated in the following studies.

3.7.2. *Impacts of Suprathermal Hydrogen Atoms on the Abundance of Glycine*

We compared the formation rate of glycine in the same way as the Fast Model. In the Slow Model, glycine is mainly built via the reaction of "s-CH_2NH_2 + s-COOH," as in the Fast Model. The formation rate of glycine in the "Fast + H^* Model" was highest in (4–5) $\times$ 10^4 yr since the beginning of the warm-up phase, with its value of between $\sim 10^{-11}$ and 10^{-12} cm^{-3} s^{-1}. This formation rate was much higher than that of the Fast Model if H^* is available.

The "Fast + H^* Model" showed that the abundance of glycine on grains was as high as $\sim 1 \times 10^{-8}$. If we excluded the reaction of "s-H^* + s-CO_2," the simulated fractional abundance of glycine was almost the same as the Fast Model. This dramatic increase of glycine in the "Fast + H^* Model" is due to the efficient formation of the COOH radical on the grains via "s-H^* + s-CO_2." Although we have included superthermal hydrogen atoms in a very simple way, it is apparent that H^* would have a strong impact on the hot core chemistry. The suprathermal hydrogen atoms may be potentially important for glycine chemistry, and we suggest to investigate the

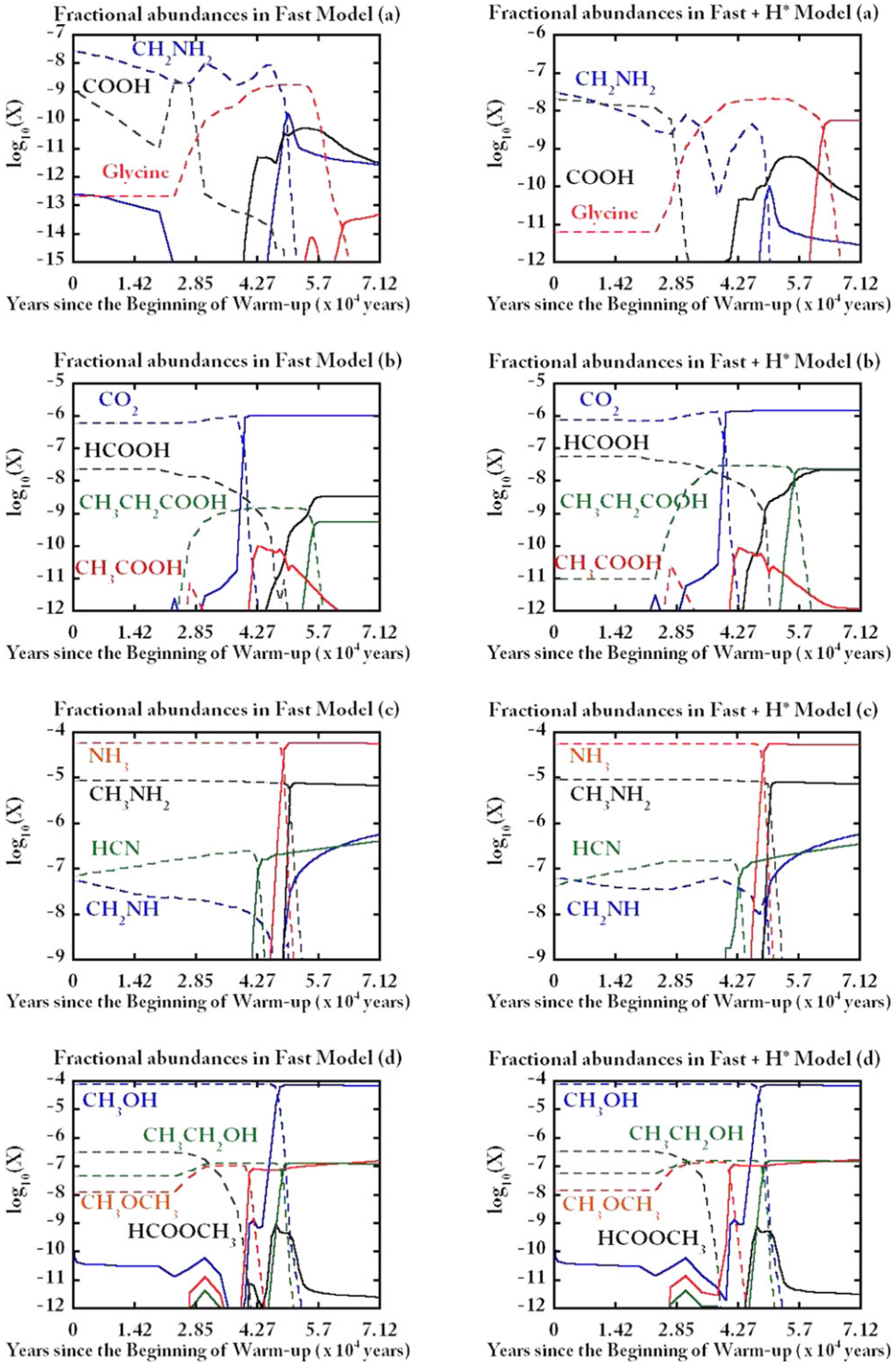

Figure 10. Time evolution of the fractional abundances of important species for the Fast Model and the "Fast + H^* Model," shown with different colors. The solid and dotted lines, respectively, represent the abundances in gas phase and on grains (surface and mantle). The time of zero corresponds to the beginning of the warm-up phase.

efficiency of suprathermal hydrogen atoms via theoretical and/or experimental studies. We will discuss the impact of the suprathermal hydrogen atoms on other COMs in the following subsection.

3.7.3. Implication of the H^* Chemistry on the Other COMs

We showed the chemical composition for the selected COMs in Figure 10, for the Fast Model and the "Fast + H^* Model." The time of zero corresponds to the beginning of the warm-up phase. The solid and dotted lines, respectively, represent the abundances in gas phase and on grains (surface and mantle).

Figure 10 suggests that the suprathermal hydrogen atoms do not change the abundance of simple molecules, such as CH_4, CO, CO_2, and H_2O, and COMs, such as CH_3OH, $HCOOCH_3$, CH_3OH, and CH_3NH_2. However, with the reaction of "s-CO_2 + s-H^*," the abundance of the COOH radical has

Table 9
The Peaks of the Simulated Abundances for the Fast Model and the "Fast + H* Model"

	Fast Model						Fast + H* Model					
	Gas		Surface		Mantle		Gas		Surface		Mantle	
Species	X	T (K)	X	T (K)	X	T (K)	X	T (K)	X	T (K)	X	T (K)
CH_3	2.5 (−6)	400	7.5 (−13)	10	4.0 (−11)	10	2.5 (−6)	400	1.4 (−12)	10	7.8 (−11)	10
NH_2	4.1 (−9)	400	7.4 (−13)	10	3.6 (−11)	10	4.0 (−9)	400	7.0 (−13)	10	3.4 (−11)	10
CN	3.2 (−10)	90	1.5 (−16)	44	9.2 (−15)	10	2.1 (−10)	90	2.3 (−16)	33	1.8 (−14)	44
OCH_3	2.4 (−9)	125	1.5 (−8)	10	9.2 (−7)	10	1.6 (−9)	125	1.8 (−8)	10	1.1 (−6)	10
CH_2OH	5.1 (−11)	132	4.8 (−9)	10	2.9 (−7)	10	3.4 (−11)	132	6.0 (−9)	10	3.7 (−7)	10
HOCO	5.2 (−11)	167	4.2 (−11)	19	2.6 (−9)	19	6.0 (−10)	177	3.6 (−10)	10	2.2 (−8)	10
CH_2NH_2	1.7 (−10)	132	4.6 (−10)	10	2.8 (−8)	10	9.9 (−11)	132	5.4 (−10)	10	3.3 (−8)	10
H_2O	2.4 (−4)	400	5.3 (−6)	125	2.3 (−4)	103	2.4 (−4)	400	5.3 (−6)	125	2.3 (−4)	103
CO	4.4 (−6)	400	7.3 (−9)	19	4.5 (−7)	19	4.9 (−6)	400	8.2 (−9)	19	5.1 (−7)	19
H_2CO	1.7 (−6)	224	3.9 (−8)	10	2.4 (−6)	10	2.3 (−6)	207	4.7 (−8)	10	2.9 (−6)	10
CH_3OH	7.3 (−5)	125	1.3 (−6)	33	7.7 (−5)	11	7.3 (−5)	125	1.4 (−6)	33	7.6 (−5)	11
CO_2	1.0 (−6)	132	1.7 (−8)	59	9.7 (−7)	59	1.4 (−6)	132	2.4 (−8)	59	1.2 (−6)	44
O_2	5.3 (−9)	68	3.0 (−13)	10	1.8 (−11)	10	9.1 (−9)	68	1.1 (−12)	10	6.9 (−11)	10
O_3	7.9 (−11)	68	4.4 (−12)	25	2.7 (−10)	25	3.3 (−10)	68	1.3 (−11)	33	8.1(−10)	33
HCN	3.9 (−7)	400	4.3 (−9)	73	2.4 (−7)	73	3.4 (−7)	400	2.7 (−9)	73	2.1 (−7)	68
HNC	4.9 (−8)	97	3.2 (−10)	84	1.8 (−8)	84	3.3 (−8)	90	3.2 (−10)	84	3.1 (−8)	84
CH_4	3.5 (−5)	33	5.7 (−7)	19	3.5 (−5)	19	3.4 (−5)	33	5.7 (−7)	19	3.5 (−5)	19
NH_3	5.7 (−5)	141	1.2 (−6)	117	5.6 (−5)	14	5.4 (−5)	141	1.1 (−6)	117	5.3 (−5)	14
C_2H_2	1.3 (−7)	400	7.9 (−10)	59	4.4 (−8)	59	1.3 (−7)	400	9.8 (−10)	59	4.2 (−8)	44
C_2H_4	5.0 (−7)	400	3.2 (−9)	59	1.8 (−7)	59	5.8 (−7)	400	3.9 (−9)	59	1.7 (−7)	44
C_2H_6	1.8 (−7)	59	5.0 (−9)	14	3.1 (−7)	14	1.6 (−7)	59	5.0 (−9)	14	3.1 (−7)	14
HNO	5.8 (−9)	79	1.0 (−9)	10	6.3 (−8)	10	3.9 (−9)	73	1.6 (−9)	10	1.0 (−7)	10
NO	3.6 (−8)	125	6.0 (−10)	10	3.7 (−8)	10	3.3 (−8)	125	9.6 (−10)	10	5.9 (−8)	10
OCN	1.9 (−10)	103	7.1 (−14)	10	4.4 (−12)	10	1.9 (−10)	90	6.2 (−13)	10	3.7 (−11)	10
SO	1.1 (−8)	73	2.9 (−10)	33	1.6 (−8)	33	1.4 (−8)	73	3.9 (−10)	33	2.2 (−8)	33
SO_2	3.7 (−9)	400	6.5 (−12)	33	3.6 (−10)	33	4.2 (−9)	400	1.6 (−11)	33	7.3 (−10)	33
NH_2CHO	1.8 (−6)	400	4.0 (−10)	136	2.3 (−8)	19	1.9 (−6)	400	4.5 (−10)	19	2.8 (−8)	19
NH_2OH	1.5 (−6)	158	6.8 (−7)	132	1.5 (−6)	25	2.0 (−6)	158	8.9 (−7)	136	2.1 (−6)	33
CH_3CN	6.2 (−9)	307	8.9 (−11)	97	4.9 (−9)	97	4.7 (−9)	307	7.0 (−11)	97	4.1 (−9)	97
CH_2NH	5.6 (−7)	400	1.0 (−9)	132	5.3 (−8)	10	5.7 (−7)	400	2.1 (−9)	132	6.3 (−8)	90
CH_3NH_2	7.4 (−6)	149	3.0 (−6)	132	8.3 (−6)	11	8.0 (−6)	149	3.0 (−6)	132	8.9 (−6)	11
NH_2CH_2COOH	4.6 (−14)	400	1.2 (−9)	163	1.6 (−9)	117	5.5 (−9)	293	1.4 (−8)	167	1.4 (−7)	117
HC_3N	2.6 (−9)	400	1.1 (−11)	97	5.8 (−10)	97	1.5 (−9)	400	4.0 (−12)	90	1.7 (−10)	90
CH_2CHCN	3.9 (−9)	90	3.9 (−10)	97	2.2 (−8)	97	4.8 (−9)	400	4.3 (−10)	97	2.9 (−8)	97
CH_3CH_2CN	4.8 (−8)	125	6.3 (−10)	103	3.5 (−8)	103	2.5 (−8)	125	2.8 (−10)	33	1.6 (−8)	103
CH_3CH_2OH	1.2 (−7)	136	2.4 (−9)	117	1.2 (−7)	44	1.5 (−7)	136	3.0 (−9)	117	2.5 (−7)	68
CH_3CHO	4.2 (−9)	400	1.8 (−11)	10	1.1 (−9)	10	4.3 (−9)	400	2.6 (−11)	10	1.6 (−9)	10
CH_3COCH_3	2.8 (−9)	400	3.5 (−13)	68	2.0 (−11)	59	2.4 (−9)	400	5.9 (−13)	68	1.2 (−8)	68
$HCOOCH_3$	8.7 (−10)	110	4.9 (−9)	10	3.0 (−7)	14	7.4 (−10)	110	5.2 (−9)	19	3.2 (−7)	19
CH_3OCH_3	1.5 (−7)	400	1.8 (−9)	44	1.0 (−7)	44	1.7 (−7)	400	2.4 (−9)	68	2.3 (−7)	68
$(CH_2OH)_2$	5.4 (−14)	248	4.1 (−14)	192	6.0 (−14)	79	2.6 (−13)	248	2.0 (−13)	192	4.7 (−14)	73
HCOOH	3.4 (−9)	314	3.6 (−10)	10	2.2 (−8)	10	2.2 (−8)	286	9.0 (−10)	14	5.5 (−8)	14
CH_3COOH	1.0 (−10)	84	1.1 (−13)	25	6.7 (−12)	25	8.5 (−11)	84	3.9 (−13)	25	1.2 (−11)	25
NH_2COOH	2.1 (−11)	207	3.9 (−11)	163	5.8 (−11)	117	1.4 (−10)	207	1.2 (−10)	163	1.9 (−10)	117
CH_3OCOOH	1.0 (−9)	182	6.6 (−10)	145	1.1 (−9)	44	1.3 (−8)	182	8.9 (−9)	145	5.4 (−8)	68
$CH_2OHCOOH$	9.1 (−10)	242	7.0 (−10)	192	9.8 (−10)	44	1.2 (−8)	242	9.5 (−9)	192	7.3 (−8)	68
C_2H_5COOH	5.4 (−10)	207	9.5 (−10)	163	1.4 (−9)	103	2.3 (−8)	213	2.0 (−8)	163	1.7 (−7)	84

Note. The peak of the fractional abundances and the temperature of grains at that moment were summarized. The notation of "a (b)" represents a $\times 10^b$.

increased by more than a factor of 10. As a result, the abundance of molecules containing the carboxyl group (i.e., HCOOH, CH_3COOH, CH_3CH_2COOH, NH_2CH_2COOH) has increased. We note that the molecules discussed in Suzuki et al. (2017), CH_3OH, $HCOOCH_3$, CH_3OCH_3, $(CH_3)_2CO$, NH_2CHO, NH_2CHO, CH_2CHCN, and CH_2NH, are not sensitive to the addition of H^*, suggesting that the "Fast + H^* Model" is able to reproduce the observed abundance in the same manner as our previous model (Suzuki et al. 2017). We summarized the peak abundances of important species in Table 9, which showed the trend that the abundances of carboxyl groups were enhanced compared with the other species. The species with the carboxyl group were mainly formed on grains via the radical–radical reactions with the COOH radical. We suggest that the observations of these species toward various star-forming regions would be a key to discussing the importance of suprathermal hydrogen atoms.

3.7.4. Dependence of the Binding Energy of H^*

One of the essential parameters to determine the significance of H^* would be the binding energy. Lowering binding energy

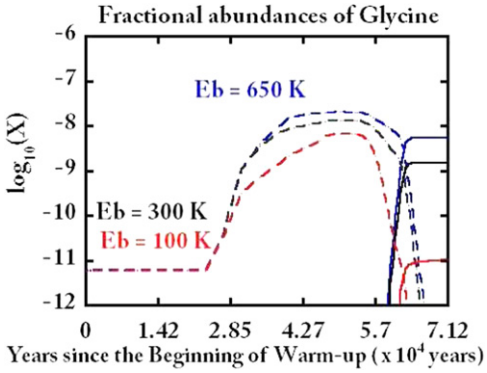

Figure 11. Abundance of glycine in the gas phase and on grains, with different binding energies. The solid and dotted lines, respectively, represent the abundances in the gas phase and on grains (surface and mantle).

will allow the H^* atom to diffuse rapidly on grains, while the timescale to reside on the grain surface will become short. In the above section, we assumed that the binding energy of H^* is the same as that of the usual H atom; however, its extra kinetic energy would increase the opportunity for H^* to move, making the binding energy much smaller than usual the H atom. Despite the importance of this, the value of the best binding energy of H^* is not known. It has to be carefully determined considering the frequency dependency of UV flux inside the cores. In this subsection, we show the effect of binding energy on the abundance of glycine.

In Figure 11, we showed the abundances of glycine in the gas phase and on grains (surface and mantle), using the solid and dotted lines, respectively. In this modeling, we used the different binding energies of 650, 300, and 100 K, and its diffusion energy was given as 40% of its binding energy. With the binding energy of 650 K, the peak abundance of glycine on grains is 2.0×10^{-8}, while they are 1.3×10^{-8} and 6.5×10^{-9}, respectively, with the binding energies of 300 and 100 K. The peak gas-phase abundances of glycine are 5.5×10^{-9}, 1.5×10^{-9}, and 2.1×10^{-11}, respectively, with the binding energies of 650, 300, and 100 K. This result suggests that the smaller binding energy of H^* will decrease the abundance of glycine on grains owing to more efficient thermal evaporation than the usual H atom. Detailed studies regarding kinetics of H^* would be required to further promote the knowledge of the formation of glycine and to predict its reliable abundance by chemical modeling studies.

4. Conclusion

The main results of this paper can be summarized as follows:

1. With the updated gas-grain chemical network and binding energies of the related species along with glycine, our model predicts a peak gas-phase glycine abundance of the order of 10^{-14}, which is almost a factor of 100 lower than that in Garrod (2013). The nondetection of glycine toward Sgr B2(N) and other high-mass star-forming regions (Kuan et al. 2003; Snyder et al. 2005) could then be explained by noncomplete desorption of this species in these sources.
2. We investigated the importance of newly suggested formation processes of glycine. We found that on the grains, glycine is mostly formed by the reaction s-CH_2NH_2 + s-COOH as previously suggested by Garrod (2013) with his fast warm-up model. However, with a glycine binding energy of 13,000 K, glycine is quickly destroyed on the grains by radicals, and the gas-phase reactions play a major role. The formation process of glycine and its precursors strongly depend on its binding energy, which should be explored in detail in future work. In addition, chemistry of NH_2OH should be investigated to understand the validity of gas-phase formation of glycine.
3. Once glycine is thermally evaporated, it is destroyed in the gas phase by positive ions and radicals. Therefore, the hot cores in the early evolutionary phase would be preferable targets for future glycine surveys.
4. We developed a very simple model including suprathermal hydrogen atoms, which is expected to be formed via photodissociation processes of UV photons and/or cosmic rays. We found that these suprathermal hydrogen atoms can increase the abundance of the COOH radical by more than a factor of 10, penetrating the activation barrier associated with the reaction of "s-H + s-CO_2" on the grain surface. Although the COOH radical was believed to be formed via the destruction of HCOOH, we suggest that the hydrogenation of CO_2 is the dominant source for the COOH radical.
5. The addition of suprathermal hydrogen atoms has a strong impact on the abundance of molecules containing the carboxyl group. Our model predicted that not only glycine but also other molecules with the carboxyl group, such as HCOOH, CH_3COOH, and CH_3CH_2COOH, would increase with the reactions of suprathermal hydrogen atoms. Astronomical observations of these species would be keys to discussing the effectiveness of the reactions with suprathermal hydrogen atoms.

We thank Dr. Hideko Nomura and staff at Bordeaux University for fruitful discussions. This study was supported by the Astrobiology Program of National Institutes of Natural Sciences (NINS) and by the JSPS KAKENHI Grant Numbers JP15H03646 and JP14J03618. V.W. acknowledges the European Research Council (3DICE, grant agreement 336474) and the CNRS program "Physique et Chimie du Milieu Interstellaire" (PCMI) co-funded by the Centre National d'Etudes Spatiales (CNES). L.M. acknowledges support from the NASA postdoctoral program. A portion of this research was carried out at the Jet Propulsion Laboratory, California Institute of Technology, under a contract with the National Aeronautics and Space Administration. This paper makes use of SAO/NASA Astrophysics Data System (ADS). Japanese Virtual Observatory (JVO) project, and The Astronomy Data Center (ADC).

ORCID iDs

Taiki Suzuki https://orcid.org/0000-0003-3278-2513
Liton Majumdar https://orcid.org/0000-0001-7031-8039
Masatoshi Ohishi https://orcid.org/000-0003-2775-7487
Masao Saito https://orcid.org/0000-0003-0769-8627
Tomoya Hirota https://orcid.org/0000-0003-1659-095X
Valentine Wakelam https://orcid.org/0000-0001-9676-2605

References

Altwegg, K., Balsiger, H., Bar-Nun, A., et al. 2016, Sci, 2, e1600285
Andersson, S., & van Dishoeck, E. F. 2008, A&A, 491, 907

Barrientos, C., Redondo, P., Largo, L., Rayón, V. M., & Largo, A. 2012, ApJ, 748, 99
Biver, N., Bockelée-Morvan, D., Moreno, R., et al. 2015, SciA, 1, e1500863
Blagojevic, V., Petrie, S., & Bohme, D. K. 2003, MNRAS, 339, L7
Boogert, A. A., Gerakines, P. A., & Whittet, D. C. 2015, ARA&A, 53, 541
Ceccarelli, C., Loinard, L., Castets, A., Faure, A., & Lefloch, B. 2000, A&A, 362, 1122
Chabot, M., Bero, K., Gratier, P., Jallat, A., & Wakelam, V. 2013, ApJ, 771, 90
Chang, Q., Cuppen, H. M., & Herbst, E. 2007, A&A, 469, 9730
Charnley, S. B., & Rodger, S. D. 2005, in IAU Symp. 231, Astrochemistry: Recent Successes and Current Challenges, ed. D. C. Lis, G. A. Blake, & E. Herbst (Cambridge: Cambridge Univ. Press), 237
Cuppen, H. M., Walsh, C., Lamberts, T., et al. 2017, SSRv, 212, 1
Ehrenfreund, P., Irvine, W., Becker, L., et al. 2002, RPPh, 65, 1427
Favre, C., Pagani, L., Goldsmith, P. F., et al. 2017, A&A, 604, L2
Garrod, R. T. 2013, ApJ, 765, 60
Garrod, R. T., Wakelam, V., & Herbst, E. 2007, A&A, 467, 1103
Green, S. D., Bolina, A. S., Chen, R., et al. 2009, MNRAS, 398, 357
Güver, T., & Özel, F. 2009, MNRAS, 400, 4
Halfen, D. T., Iyushin, V. V., & Ziurys, L. M. 2013, ApJ, 767, 66
Hirota, T., Kim, M. K., Kurono, Y., & Honma, M. 2015, ApJ, 801, 82
Holtom, P. D., Bennett, C. J., Osamura, Y., Mason, N. J., & Kaiser, R. I. 2005, ApJ, 626, 940
Ikeda, M., Ohishi, M., Nummelin, A., et al. 2001, ApJ, 560, 792
Jonusas, M., & Krim, L. 2016, MNRAS, 450, 1977
Kuan, Y. J., Charnley, S. B., Huang, H. C., Tseng, W. L., & Kisiel, Z. 2003, ApJ, 593, 848
Lee, C.-W., Kim, J.-K., Moon, E.-S., Minh, Y.-C., & Kang, H. 2009, ApJ, 697, 428
Liu, S.-Y., Girart, J. M., Remijan, A., & Snyder, L. E. 2002, ApJ, 576, 255
Loison, J.-C., Wakelam, V., & Hickson, K. M. 2014a, MNRAS, 443, 398
Loison, J.-C., Wakelam, V., Hickson, K. M., Bergeat, A., & Mereau, R. 2014b, MNRAS, 437, 930
Majumdar, L., Das, A., Chakrabarti, S. K., & Chakrabarti, S. 2013, NewA, 20, 15
Mehringer, D. M., Snyder, L. E., & Miao, Y. 1997, ApJL, 480, L71
Muñoz Caro, G. M., Meierhenrich, U. J., Schutte, W. A., et al. 2002, Natur, 416, 403
Nishi, N., Shinohara, H., & Okuyama, T. J. 1984, ChPh, 80, 3898
Nomura, H., & Millar, T. J. 2004, A&A, 414, 409
Pagani, L., Favre, C., Goldsmith, P. E., et al. 2017, A&A, 604, A32
Prasad, S. S., & Tarafdar, S. P. 1983, ApJ, 267, 603
Pulliam, R. L., McGuire, B. A., & Remijan, A. J. 2012, ApJ, 751, 1
Rodgers, S. D., & Charnley, S. B. 2001, ApJ, 546, 324
Ruaud, M., Loison, J. C., Hickson, K. M., et al. 2015, MNRAS, 447, 4004
Ruaud, M., Wakelam, V., & Hersant, F. 2016, MNRAS, 459, 3756
Singh, A., Misra, S. A., & Tandon, P. 2013, Astron, 13, 912
Snyder, L. E., Lovas, F. J., Hollis, J. M., et al. 2005, ApJ, 619, 914
Suzuki, T., Mahumdar, L., Ohishi, M., et al. 2017, ApJS, 273, 3
Suzuki, T., Ohishi, M., Hirota, T., et al. 2016, ApJ, 825, 79
Theule, P., Borget, F., Mispelaer, F., et al. 2011, A&A, 534, A64
Tzvetkov, G., Ramsey, M. G., & Netzer, F. P. 2004, CPL, 397, 392
Wakelam, V., Herbst, E., & Selsis, F. 2006, A&A, 451, 551
Wakelam, V., Loison, J.-C., Herbst, E., et al. 2015, ApJS, 217, 20
Wakelam, V., Loison, J. C., Mereau, R., & Ruaud, M. 2017, MolAs, 6, 22
Walsh, C., Millar, T. J., Nomura, H., et al. 2014, A&A, 563, A33
Woon, D. E. 2002, ApJL, 571, L177
Zhu, R. S., Diau, E. G. W., Lin, M. C., & Mebel, A. M. 2001, JPCA, 105, 11249